Run-time optimization of a radiation driven crown fire model
by Patrick Timothy Call

A thesis submitted in partial fulfillment of the requirements for the degree of Master of Science in Mechanical Engineering
Montana State University

Abstract:
A numerical model of the behavior of wildland forest fires is studied. The model predicts spread rate, flame geometry, and intensity of a crown fire using the radiation transport equation. This thesis presents dimensional analyses applying the physics of fire to justify the model assumptions, and introduces a closure scheme that expedites the model convergence. The closure scheme minimizes the number of outer iterations the model performs by efficiently converging to a consistent solution. It was discovered that the number of outer iterations can be minimized through the use of a linear approximation scheme. The selected closure scheme has performed well in the limited number of test cases for which data are available.

RUN-TIME OPTIMIZATION OF A RADIATION DRIVEN CROWN FIRE MODEL

by

Patrick Timothy Call

A thesis submitted in partial fulfillment
of the requirements for the degree

of

Master of Science

in

Mechanical Engineering

MONTANA STATE UNIVERSITY
Bozeman, Montana

April 1997

APPROVAL

of a thesis submitted by

Patrick Timothy Call

This thesis has been read by each member of the thesis committee and has been found to be satisfactory regarding content, English usage, format, citations, bibliographic style, and consistency, and is ready for submission to the College of Graduate Studies.

Frank Albini _____ (Signature) 14 Apr '97 Date

Approved for the Department of Mechanical and Industrial Engineering

Vic Cundy _____ (Signature) 4/14/97 Date

Approved for the College of Graduate Studies

Robert Brown _____ (Signature) 4/28/97 Date

STATEMENT OF PERMISSION TO USE

In presenting this thesis in partial fulfillment of the requirements for a master's degree at Montana State University - Bozeman, I agree that the Library shall make it available to borrowers under rules of the Library.

If I have indicated my intention to copyright this thesis by including a copyright notice page, copying is allowable only for scholarly purposes, consistent with "fair use" as prescribed in the U.S. Copyright Law. Requests for permission for extended quotation from or reproduction of this thesis in whole or in parts may be granted only by the copyright holder.

Signature Patricia Call

Date April 14, 1997

ACKNOWLEDGMENT

The author wishes to express his appreciation to the USDA Forest Service, Intermountain Research Station for research joint venture agreement INT-95082-RJVA and to the Canadian Forest Service for its support under Green Plan research contribution "A physical model for crown fire behavior."

TABLE OF CONTENTS

LIST OF TABLES

TABLE

LIST OF FIGURES

FIGURE

NOMENCLATURE

α	thermal diffusivity	m^2/s
b	width of flame base in a line fire	m
B	Stephan-Boltzman constant	5.67×10^{-8} $W/m^2/K^4$
β	fraction of volume filled with solids in fuel layer	
Bi	Biot number of fuel particle	
C	reaction rate coefficient, opacity parameter	
C_p	specific heat	kJ/kg/K
δ	layer depth	m
d	diameter	m
D	depth of burning zone	m
Fr	Froude number	
g	acceleration of gravity	m/s^2
γ	tilt angle	
h	convective heat transfer coefficient	$W/m^2/K$
H	height of flame	m
H_a	heat-release rate of fuel per unit mass of air	W/kg
H_c	heat of combustion for the fuel	KJ/kg
I	line intensity of fire	W/m
k	thermal conductivity	W/m/K

NOMENCLATURE - Continued

l', m', n'	direction cosines	
L	flame length	m
Nu	Nusselt number	
P_f	power of the fire	W/m^2 ($Btu/ft^2/s$)
P_w	power of the wind	W/m^2 ($Btu/ft^2/s$)
ρ	mass density	kg/m^3
ρ_o	oven dry density of fuel particles	kg/m^3
ρ_{wt}	weight density	N/m^3
q_1, q_2, q_i	three regimes of heat absorption in fuel bed	W/m^3
$\dot{Q}'$	heat transfer rate per unit length	W/m
Q_d^*	dimensionless buoyancy flux	
$\dot{Q}_o$	heat release rate of the fire	W
$\dot{Q}_{rad}'''$	net rate of absorption of energy in fuel bed	W/m^3
R	rate of spread for flame geometry	m/s
RR	reaction rate	s^{-1}
R_{mix}	air / flame fluid mixing rate	s^{-1}
s	distance in direction of radiation ray	m
S	speed of ignition isotherm	m/s

NOMENCLATURE - Continued

S_L	burning velocity	m/s
t_r	thermal relaxation time	s
T	temperature of particle in fuel bed	K
T_a	ambient air temperature	K
T_b	temperature of boiling point of water	K
T_B	temperature of burning zone	K
T_f	final temperature	K
T_i	ignition temperature	K
τ_{burn}	time to burn a particle	s
τ_{fl}	fluid transit time	s
τ_{mix}	characteristic mixing time	s
τ_r	characteristic heating time	s
u	horizontal component of velocity	m/s
$\bar{U}$	mean free stream wind velocity	m/s
U_c	wind velocity at crown top	m/s
V	total velocity	m/s
w	vertical component of velocity	m/s
w_c	mass of fuel consumed per unit area	kg/m^2
w_o	dry fuel loading of a layer	kg/m^2

ABSTRACT

A numerical model of the behavior of wildland forest fires is studied. The model predicts spread rate, flame geometry, and intensity of a crown fire using the radiation transport equation. This thesis presents dimensional analyses applying the physics of fire to justify the model assumptions, and introduces a closure scheme that expedites the model convergence. The closure scheme minimizes the number of outer iterations the model performs by efficiently converging to a consistent solution. It was discovered that the number of outer iterations can be minimized through the use of a linear approximation scheme. The selected closure scheme has performed well in the limited number of test cases for which data are available.

CHAPTER 1

INTRODUCTION

For many decades, research has been conducted in an attempt to better understand the phenomena of fire. As one of mankind's first tools, fire is an invaluable source of energy and a tremendous means of destruction. Each year, fire claims on average 10-20 lives per million people population (Cox 1995). This, along with the staggering impact fire directly and indirectly has on the economy, is a motivation for scientists and engineers to try to better understand physical principles governing fire.

The fires responsible for loss of life and destruction of property can be classified into two major categories: structural and wildland. Structural fires occur in buildings or other man-made structures, and are generally confined by artificial boundaries. Wildland fires burn in grass, brush, timber or other forms of vegetation, and are not necessarily confined by artificial boundaries. With the aid of wind and topography, free-burning wildland fires can create a tremendous impact (although not always bad) on the vegetation and wildlife in the area.

Wildfires can be categorized into three major groups: ground fires, surface fires, and crown fires. Ground fires burn the organic layers found below the surface and generally creep at a very slow pace (Albini, 1984). Surface fires burn the vegetation on or near the surface and have the potential to move at very high speeds. Surface fires

consume fuels that include litter, grasses, and shrubs, along with the larger dead fall and live juvenile trees. A crown fire burns the foliage and branches in the tops of trees. Crown fires perpetuate their motion by moving from treetop to treetop, although there usually is a surface fire occurring simultaneously with the crown fire.

The most destructive of these three types of wildland fires is the crown fire. Crown fires account for less than 10 percent of the total wildland fires, but burn 90 percent of the total acreage (Albini and Stocks, 1986). All crown fires start out as surface fires with all the burning taking place below the crown. If conditions such as ample wind and dense surface vegetation are met, a surface fire can climb into the crown and continue its motion in the crown (Van Wagner, 1977).

Fire management personnel are interested in controlling and even harnessing wildland fires, thus continuing efforts are in progress to create models that can predict the speed, intensity, and direction of motion of wildland fires. Several models exist today that attempt to solve the problem of modeling a wildland fire. These models are primarily empirical in nature. They consider wind, terrain, moisture content of the fuel, and type of fuel as parameters. These models use controlled experimental fires in which all the fuel characteristics are determined prior to ignition, and the speed, shape, and size are recorded after the burn. With enough experimental data, a 'black box' model can be created that takes inputs and then estimates a solution using predicted fire behavior. Empirical models are approximate and do not attempt to explain the fluid flow processes and heat transfer mechanisms involved in a wildland fire. Understanding these processes may ultimately lead to broadly applicable models.

The phenomenology of free burning wildland fires is described in Albini (1984; 1992). Free-burning fires spread by igniting new fuel at the periphery. Vegetation fuels vary in size, moisture content, and compactness, so that the finest fuels are the agents of spread. They are most readily ignited and burn out most rapidly. Only fuels up to approximately a few millimeters in diameter participate in the spread process. Other components may interfere with the heat transfer process and add to heat required for ignition, but contribute little to the heat release.

The ignition of the fuel is controlled by piloted ignition of volatile pyrolyzate, the combustible gases released by thermally decomposing vegetable matter. Gases burn upon mingling with oxygen, releasing heat energy in the form of radiation and hot gaseous products of combustion. Radiation from the sooty flames of natural fires is almost entirely due to small (approximately less than 10^{-5} meters in diameter) solid particles in the flame that are heated by contact with the hot products of gaseous combustion and by glowing combustion of the particles.

Small vegetation fuel particles (leaves, small twigs, bark flakes, etc.) once ignited burn on the order of 10 seconds before they are reduced to mineral ash. The heat released in this process causes the mixture of gases (pyrolyzate, air, and gaseous combustion products) to rise buoyantly, creating the visible structure we identify as the flame. This structure, reaching from the surface to above the top of the highest fuel layer involved in the fire, radiates vigorously. In a crown fire, where flames may extend tens of meters above the tops of trees, exposed skin can be promptly blistered at a distance of 100 meters.

If the fire advances at a steady rate, then during the combustion of ignited fine fuels, enough heat must be transferred to the same mass of unignited fuel particles ahead of the fire front to raise their temperatures to the piloted ignition temperature, about 600K (Stockstad, 1975). In typical conifer tree crowns, the dry mass of live foliage per unit volume is on the order of 200 gm/m^3. These particles are roughly cylindrical, with length over diameter ratios very much larger than unity. It will be shown below that they can be modeled as thermally thin, or isothermal. If the foliage is thermally thin and contains water mass approximately equal to its dry mass, then the energy required simply to boil away the water is on the order of 0.5 MJ/m^3. So, if the fire front is advancing at, for example, 0.3 m/s, this is equivalent to a heat transfer rate of 150 kW/m^2. This clearly rules out thermal conduction; if the conductivity of air is assumed to be 0.05 W/mK, the thermal gradient would have to be 3×10^6 K/m. Since the maximum temperature achievable by the combustion of natural conditions is about 1500 K, the temperature difference between fuel particles at the boiling temperature of water and the hypothetical burning zone at 1500 K would have to be maintained over a fraction of a millimeter.

The required heat transfer could presumably be accomplished by convection, if the hot flame fluid passes through unignited vegetation fuel. In this work we shall be concerned with modeling the steady advance of long line fire under the influence of an aiding wind. But it will be shown below that there exists a broad regime in which the buoyant flow of the flame fluid obstructs the path of the aiding wind, allowing the free flame above the tops of the trees to stand erect, creating a zone of stagnant air immediately down stream of the burning zone. This is shown in Figure 1.

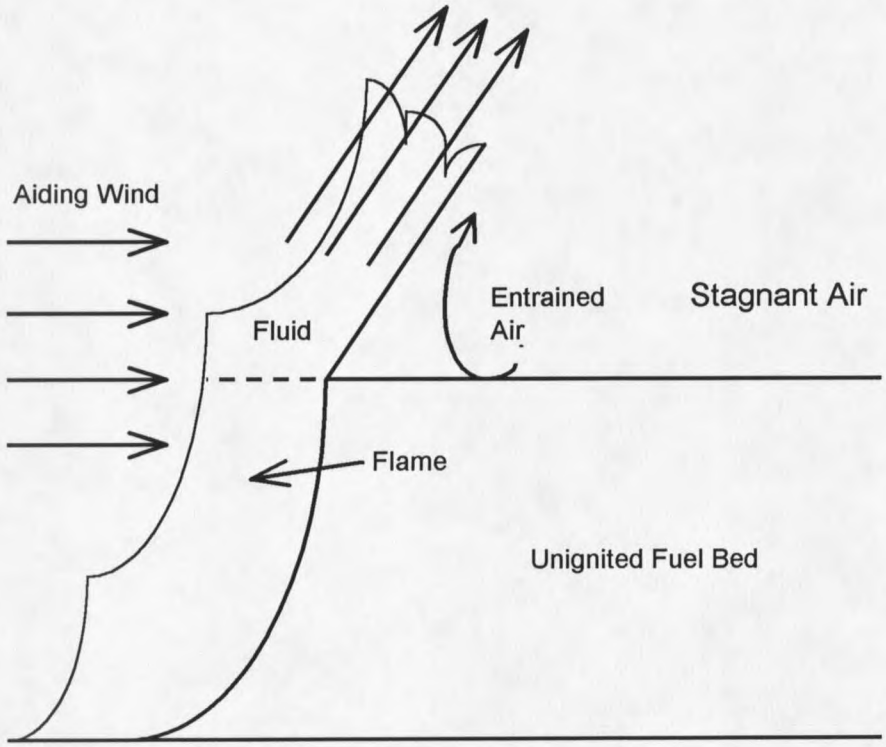

Figure 1. Air flow diagram of a free-burning fire.

In this instance, the condition being modeled, there can be no convective heat transfer to the unignited fuel because the flame fluid does not come into contact with the unignited fuel. Thus the heat transfer mechanism that causes the fire to spread is radiation, and the rate of heat transfer determines the rate of fire spread.

The fuel bed ahead of the fire can be viewed as three separate layers: surface layer, stem space layer, and crown layer (Albini, 1984). The surface layer consists of all the fuel on or near the ground and also a small portion of the duff just underneath the surface. The amount of duff contributing to the flame structure of the crown fire is only the depth the burn will reach in the initial passing of the flaming front. The remaining duff beneath this is not considered. The next layer, the stem space layer, is the area between the surface

fuels and the crown foliage. This layer is mostly comprised of boles. The top layer, the crown layer, is comprised of the small diameter fuel components along with the larger branches and boles. Each of these layers contributes to the heat energy given off in the burning zone which will determine the flame structure and hence the rate of spread of the flaming front.

A simplified fuel bed is created in order to identify the rate at which radiant heat is causing the temperature to rise in the fuel bed. There are several components used to describe the fuel. These consist of layer depth, layer opacity parameter, loading, oven dry fuel density, mineral ash fraction, moisture content, heat of combustion, and surface area to volume ratio of the fuel particles. The contributions of each fuel component to these parameters are computed according to a weighted average scheme. This scheme preserves most of the physical features of the fuel bed while combining their contributions into those of a single size class that is completely consumed by the passing fire front. This eliminates the need to classify each particle of fuel and its contribution to the flame front. The radiation driven crown fire model described by this paper uses the representative value of each of the above components as detailed in Albini (1996) and Call and Albini (in press).

Several mathematical idealizations of the situation modeled are summarized below to give an understanding of the assumptions needed to simplify the calculations. 1. The fire is modeled as a two-dimensional line fire that is aided by wind blowing in the direction of the motion of the fire. 2. The burning zone bounding surface is called the 'ignition interface', and is an isotherm at the ignition temperature, T_i. 3. The free flame is a flat

diffuse radiator. 4. The fuel bed layers are replaced by hypothetical equivalent layers made up of a single size class totally consumed by the passing of the fire. 5. The fire is characterized by spread rate and intensity, where intensity is measured as the power per unit length of the fire edge. The units of intensity in the metric system are in kW/m. 6. The incident wind field is characterized by the crown top velocity, U_c, and the log speed profile (Baughman and Albini, 1980). 7. A simplified flame structure model uses intensity, wind field and stand height to predict the flame height and tilt angle (Albini, 1981).

The two dimensional geometry of the crown fire model is illustrated in Figure 2. The spread is modeled by attaching the coordinate system to the interface, and advancing the fuel from right to left into the flame at speed S.

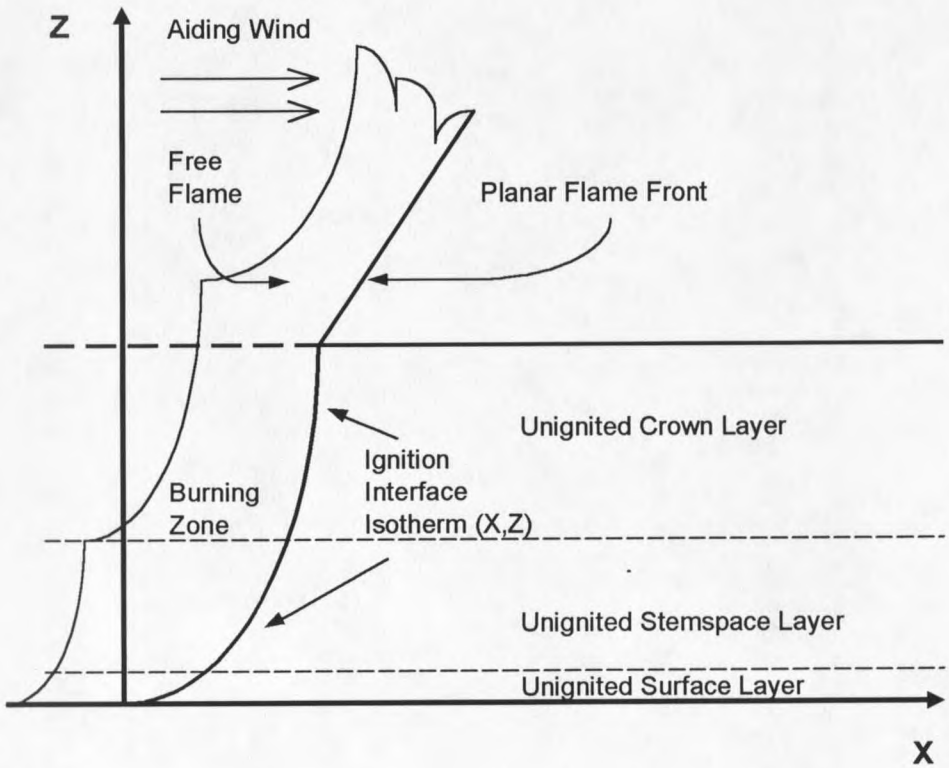

Figure 2. Geometry of flame/fuel interface.

The specific objectives of this thesis are twofold. First, to develop the physics and mathematics needed in the modeling of a radiation driven crown fire. To understand the physical mechanisms discussed briefly in this introduction, sufficient background in the temporal and spacial scales are given to support the model assumptions through the use of an order of magnitude analysis. This analysis leads into the specific development of the model by applying the governing equations of radiation heat transfer.

The model exists as FORTRAN code with four levels of iterations that are extremely process intensive. After describing the model structure, the second objective is to develop an iteration scheme that will allow the expedient convergence of the model code. This task can be accomplished either by increasing the efficiency of the iterations consuming the most time, or by minimizing the number of times the model performs these iterations. The focus of this study is to minimize the number of outer iterations the model performs which greatly decreases the time needed for convergence.

CHAPTER 2

BACKGROUND

Time Scales

Four different types of time comparisons are presented to explain the relative importance of the processes involved with a crown fire. The first time comparison is a ratio of the characteristic heating time to the thermal relaxation time which, if small enough, proves that the modeled fuel particles can be treated as thermally thin. The second comparison is the ratio of the time it takes for the fluid to transit from the base of the flame to the tip of the flame to the time it takes for the air to mix with the flame. This helps explain why the flame structure remains relatively stable as opposed to sporadic flickers of flame. The next comparison considers the time it takes to completely burn a fuel particle divided by the time for the fluid to transit the flame. This also explains how the flame maintains a stable structure. The last comparison is the ratio of the chemical reaction time to the time it takes fluid to pass through the flame from the base to the tip, also known as the Damkohler number. A very small Damkohler number will prove that the chemical reaction process need not be modeled. These four comparisons are individually analyzed below.

Characteristic heating time / thermal relaxation time

The heating characteristic time can be derived from the equation for particle heating due to convection. This equation is

$$\dot{Q}' = h\pi d(T_f - T) \tag{1}$$

where $\dot{Q}'$ is the heat transfer rate per unit length into the cylindrical fuel particle, h is the convective heat transfer coefficient, d is the diameter of the fuel particle, T is the temperature of the particle, and T_f is the final temperature. This relation can be equated to an expression for the heat storage rate in a uniform-temperature particle derived from the first law of thermodynamics. This expression is:

$$\dot{Q}' = \frac{\pi d^2}{4}\rho C_p \frac{dT}{dt} \tag{2}$$

where C_p is the specific heat of the particle and ρ is the density of the particle. When these two expressions are equated, the following differential equation is obtained:

$$\frac{dT}{dt} = \frac{4h}{\rho C_p d}(T_f - T) \tag{3}$$

The solution of this equation results in a expression that gives the exponential temperature history of a particle. This is given as:

$$\frac{T - T(0)}{T_f - T(0)} = 1 - e^{-\frac{4ht}{\rho C_p d}} \tag{4}$$

From this, the characteristic heating time is defined as:

$$\tau_h = \frac{\rho C_p d}{4h} \tag{5}$$

In this instance, the characteristic heating time is a measure of the time it takes to bring a particle of fuel to a temperature where combustion can occur.

The thermal relaxation time is the square of the characteristic dimension over the thermal diffusivity (6). This is the time a particle of fuel needs to distribute heat throughout its interior. As can be seen, this parameter is strongly dependent on the diameter.

$$t_r = \left(\frac{d}{2}\right)^2 \cdot \frac{1}{\alpha} \tag{6}$$

The relative size of these two characteristic times is very important to the assumption of thermally thin particles. It can be shown that the ratio of heating time to thermal relaxation time is the Biot number:

$$Bi = \frac{t_r}{\tau_h} \tag{7}$$

where t_r is the thermal relaxation time, and τ_h is the characteristic heating time. To show these two times are related by the Biot number, the following development is given to reduce equation (7) to the familiar expression for Biot number (9):

$$Bi = \frac{\left(\frac{d}{2}\right)^2 \cdot \frac{1}{\alpha}}{\frac{\rho \cdot C_p \cdot d}{4 \cdot h}} \tag{8}$$

$$Bi = \frac{h \cdot d}{\rho \cdot C_p \cdot \alpha} = \frac{h \cdot d}{k} \tag{9}$$

The Biot number is also equal to the Nusselt number multiplied by the ratio of the thermal conductivity of air to that of the particle (10).

$$Bi = Nu \cdot \frac{k_{particle}}{k_{air}} \tag{10}$$

The thermal conductivity values are estimated at approximately 0.045 W/mK for air, and approximately 0.1 for wood. These values can only be estimated at 600 degrees Kelvin due to the lack of experimental data for conductivity of fuel material. The Nusselt number is taken to be consistent with natural convection, 0.35, because of the lack of air movement just ahead of the fire (proof of this is given in Chapter 3). Using this relation it can be seen that the Biot number is about 0.7, implying the particles can be treated as thermally thin, or isothermal.

Time for fluid flow / time for fluid to mix

The nomenclature needed to develop this section and the following sections of the time comparisons is given in Figure 3. The figure expands upon Figure 2 by identifying the burning zone and the longitudinal depth of the burning zone, D (lower case d is always used for diameter), and the height of the fuel layer, δ. The flame height, H, is shown along with the flame length, L. These two distances are related by the tilt angle, γ. The wind is assumed to be horizontal with average speed $\bar{U}$ over the flame height.

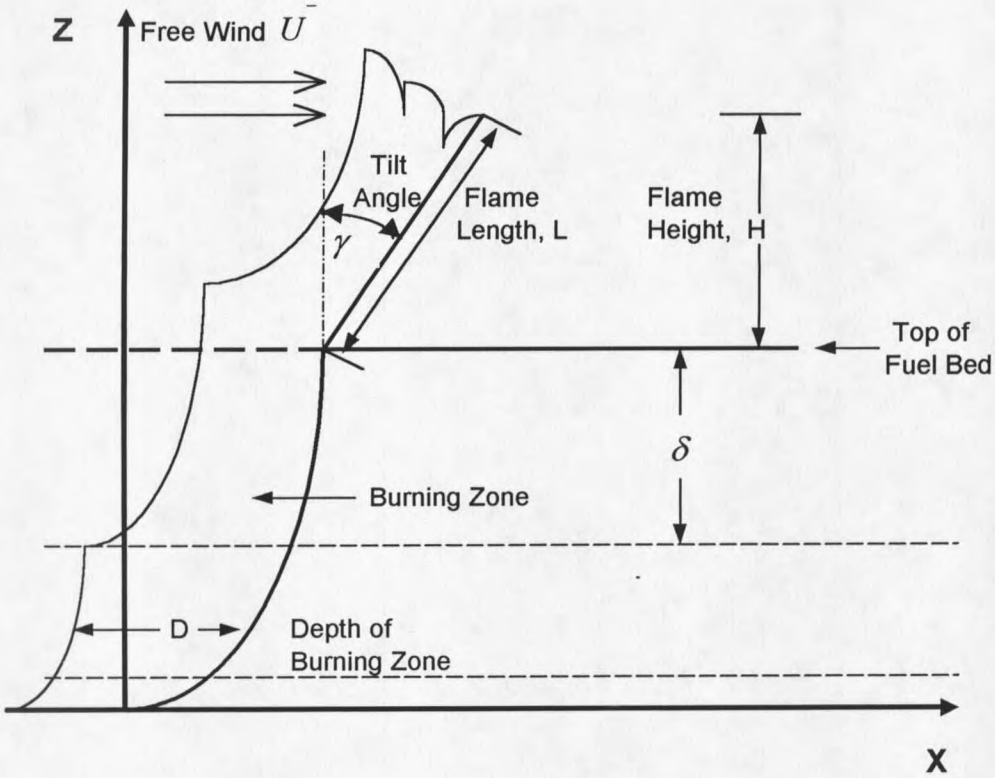

Figure 3. Geometry needed to develop the time comparisons.

The characteristic time for a fluid particle to pass from the bottom of the flame through to the tip of the flame is explained in great detail in the flame structure paper by Albini (1981). Two methods can be used to find this characteristic time. The first is to divide the height of the flame, H, by the component of the total velocity moving in the upward direction, w (11). The second is to divide the flame length, L, by the total velocity of the fluid (12). Either of these two methods could be used, but for this example the first will be shown.

Method 1: $$\tau_{fl} = \frac{H}{w} \tag{11}$$

Method 2: $$\tau_{fl} = \frac{L}{V} = \frac{L}{\sqrt{u^2 + w^2}} \tag{12}$$

The tilt angle of the flame is needed to find the component of the velocity in the upward direction. Assuming that the average flame fluid streamlines are very nearly straight (Albini, 1981), the horizontal velocity, u, divided by the vertical velocity, w, is equal to the tangent of the tilt angle γ (13).

$$\tan\gamma = \frac{u}{w} = const. \tag{13}$$

The expression for tan γ given in Albini (1981) is:

$$\tan^2\gamma = \frac{3\bar{U}^2}{2gH} \tag{14}$$

where g is the acceleration of gravity and H is the flame height. Using these two expressions, the average vertical velocity can be solved in terms of the flame height (15).

$$w = \sqrt{\frac{2gH}{3}} \tag{15}$$

Next, the characteristic time can be found by taking the height divided by the vertical velocity. This is shown in equation (16) after substituting w into equation (11).

$$\tau_{fl} = \sqrt{\frac{3H}{2g}} \tag{16}$$

The characteristic mixing time, τ_{mix}, can be calculated by taking the reciprocal of the rate of mixing of the air with the gaseous products given off from the heating of the fuel, or pyrolyzate. The rate of mixing, R_{mix}, is approximated as (Spalding, 1976):

$$R_{mix} = C \cdot \left| \frac{du}{dz} + \frac{dw}{dx} \right| \approx C \cdot \frac{2 \cdot w}{D} \tag{17}$$

where C is a dimensionless coefficient and D is the longitudinal depth of burn of the flame front. Spalding approximated the C coefficient as 0.35. For the purpose of this calculation, the velocity gradient in the z direction can be assumed to be very small when compared to the velocity gradient in the x direction. This is because the fluid particle is rapidly accelerated in the vertical direction in a small x distance versus a small acceleration in the horizontal direction in a larger distance in z. The gradient in the x direction is further simplified as two times the vertical velocity divided by the depth of burn (Albini, 1981). The characteristic mixing time then reduces to an expression in terms of the depth of burn and the vertical velocity (18).

$$\tau_{mix} = \frac{D}{0.7w} \tag{18}$$

Once the expressions for τ_{mix} (18) and τ_{fl} (16) are found, a ratio of the two can be taken to determine if one is significantly larger than the other. Dividing the characteristic mixing time by the time for fluid flow to pass, the following expression is obtained.

$$\frac{\tau_{mix}}{\tau_{fl}} = (\frac{D}{H}) / 0.7 \tag{19}$$

This expression is meaningful because it shows qualitatively that the mixing time is the same order of magnitude as the time it takes for a particle of fluid to traverse the

flame. This is true when the depth of burn, D, is of the same order of magnitude as the flame height, H, which is the case in the crown fires this model is intended to simulate. This conclusion is significant in that it helps give meaning to the shape of the flame in a crown fire. If the mixing rate were much higher than the time it takes for the fluid flow, the flame structure would simply flicker instead of giving a consistent shape.

Time to burn particle / transit time for fluid

The time a particle of fuel needs to completely pyrolyze can be analyzed using two different methods. One method is to use a series of simplifications in an order of magnitude analysis to show that the time it takes to burn the particle is large when compared to the mixing time. The other method comes from a publication by Albini and Reinhardt (1995) where the time can be calculated from experimental equations.

The simplest way to perform an order of magnitude analysis on the burning time of a particle is to take the mixing time from equation (18) and then substitute the spread rate multiplied by the characteristic time to burn a particle. The characteristic time to burn a particle is conceptually defined as the longitudinal depth of burn divided by the speed of the fire, S. After a few steps of algebra, the following expression with the burning time divided by the mixing time is obtained:

$$\frac{\tau_{burn}}{\tau_{mix}} = \frac{0.7H}{S\tau_{fl}} \tag{20}$$

However, the ratio that is being analyzed is the burning time divided by the fluid transit time, not the burning time divided by the mixing time. Since the fluid transit time was

previously proven to be of the same order of magnitude as the mixing time, this ratio can be used to compare the time to burn the particle and the transit time for the fluid.

To determine the order of magnitude of this ratio, sample numbers can be substituted from observation of actual crown fires (Stocks, 1987). For example, if a flame height, H, of 7 meters, a spread rate, R, of 0.2 meters per second, and a τ_{fl} of 1 second is substituted into equation (20), a ratio of 25 is obtained. These numbers demonstrate that the time it takes for a fuel particle to completely burn is much greater than the time needed for the fluid to mix.

The second method for calculating the characteristic time to burn a fuel particle can be taken from Albini and Reinhardt (1995). An empirical equation is given in this publication that was developed from laboratory data. The equation is:

$$\tau_{burn} = \left(\frac{928-673}{T_F - T_C}\right)\cdot\left(\frac{\rho_o}{446}\right)\cdot\left(\frac{d}{h_{eff}}\right)\cdot(a'+Mb') \qquad (21)$$

where T_F is the fire environment temperature, T_C is the burning particle's surface temperature, ρ_o is the oven dry density of the particle, d is the diameter of the particle, h_{eff} is the effective heat transfer coefficient, and a' and b' are empirical constants. Plugging in numbers that are used for this model, τ_{burn} is approximately 10 seconds. The ratio then becomes approximately 10, which is consistent with the above findings.

The fact that the ratio τ_{burn} / τ_{fl} is of the order of 10 implies that the time to burn the particle is much larger than the transit time for the fluid. This gives a stable flame structure for the fire allowing the flame to be treated as stationary.

Time for the chemical reaction to complete / transit time for fluid

To understand the time needed for the gas phase chemical reaction to complete, the concept of flame speed is needed. The flame speed, or burning velocity, is defined as the velocity at which unburned premixed fuel and oxidizer gases travel through a stationary combustion wave in a direction perpendicular to the wave surface (Glassman, 1977). The flame is referred to as a wave in this definition due to the wave like motion of the flame as it propagates through a medium. To determine the flame speed, several approaches using different theories have been developed. Fortunately, they all lead to the same conclusion. For the purpose of this argument, the simplest derivation will be given.

The analysis first was done by Mallard and Le Chatelier (Glassman, 1977) who stated that the controlling mechanism of the flame propagation was the heat traveling back through the layers of gas. The analysis was done by dividing the flaming zone of the combustion into two regions: the region of heat transfer and the region of burning. The interface between these two regions is the point at which ignition occurs. The Mallard and Le Chatelier model assumed that the temperature increase from the ignition temperature to the final burning temperature was linear. This greatly simplified the analysis of determining the burning velocity. The result was the following expression:

$$S_L = \left(\frac{k}{\rho c_p} \cdot \frac{T_f - T_i}{T_i - T_o} \cdot \frac{d\varepsilon}{dt} \right)^{\frac{1}{2}} \tag{22}$$

where S_L is the burning velocity, k is the thermal conductivity, ρ is the density of the gas, c_p is the specific heat, and $\frac{d\varepsilon}{dt}$ is the time rate of change of the combustion product mole

fraction. This expression can be simplified even further by noting that burning velocity is directly proportional to the square root of the thermal diffusivity multiplied by the reaction rate (23).

$$S_L \sim (\alpha RR)^{1/2} \tag{23}$$

This expression can be used to obtain an estimate of the order of magnitude of the reaction rate by using nominal values for thermal diffusivity and burning velocities. Burning velocities have been experimentally shown to be 0.3 m/s to 1.4 m/s for common hydrocarbon fuels (Drysdale, 1985). Taking the burning velocity to be about 1.4 m/s and the thermal diffusivity to be 0.00008 m^2/s (Cengal and Boles, 1989), the reaction rate is on the order of 20000 s^{-1}. Taking the reciprocal of the reaction rate to be the chemical reaction time, the resulting number is on the order of 0.05 milliseconds. In a crown fire, this chemical reaction time can be taken as negligible when compared to the time it takes to move in the oxygen (air) needed for the combustion. The time it takes for fluid transit is on the order of 1.0 second, while the time it takes for the chemical reaction to complete is closer to 0.05 milliseconds. This gives a Damkohler number of 0.00005, which means the controlling mechanism is not kinetically limited.

This result has an important implication in crown fire modeling. The speed that a crown fire moves is governed by the slowest process taking place in the crown fire. Thus, one way to model the crown fires is to only model the slowest process and assume all the other processes occur, but do not affect the modeled process. In this case, all other times discussed are much larger than the chemical reaction time, so the chemical reaction time need not be modeled.

Space Scales

To obtain a feeling for the order of magnitude of the physical dimensions involved with the model, several space scales can be defined. The first space scale is the distance ahead of the fire that heat transfer from the flame will affect the fuel bed. In theory, the radiation from the flame will reach an infinite distance, but this is not practical to model. For this reason a cold boundary is defined as the location on the fuel bed where the temperature rise due to radiation is a set value. This value can be changed by the user of the model, and is typically about 20 degrees Celsius. The resulting distance is five to ten times the height of the flame above the tree stand, or on the order of 50 meters.

The next space scale is the depth of the burning zone. This was previously defined as the rate of spread of the flaming front multiplied by the time it takes for a particle to be completely consumed. The time to burn a particle was calculated to be approximately 10 to 20 seconds. The rate of spread of a crown fire has been observed to range from around 15 centimeters per second to 50 centimeters per second or more. Thus, a range for the depth of burn is 1.5 meters to 10 meters.

The radiation extinction length is the distance needed for the radiation passing through the fuel layer to be diminished in intensity by the factor e^{-1}. The optical extinction parameter (inverse of the extinction length) can readily be shown, for randomly-oriented convex fuel particles uniformly distributed, to be:

$$C = \frac{\sigma\beta}{4} \tag{24}$$

where σ is the fuel particle surface area to volume ratio and β is the fraction of volume filled with solids. β is defined in terms of the dry fuel loading, dry weight density, and the thickness of the fuel layer. This equation for β is:

$$\beta = \frac{w_o}{\rho_o \delta_{layer}} \tag{25}$$

where w_o is the the dry fuel loading in kg / m^2, ρ_o is the dry mass density, and δ_{layer} is the vertical fuel layer thickness.

The extinction length can be calculated for each layer within the fuel bed. For the purpose of this model, only the crown foliage layer will be analyzed because the radiation from the flaming front will primarily be absorbed in the crown layer. The geometry of the fuel particles in the crown layer are taken as long, thin cylinders, thus the surface area to volume ratio can be reduced to 4 over the diameter. The diameter of a typical particle is on the order of a millimeter. The dry loading of a crown layer is typically on the order of 1.0 kg / m^2, and the oven dry density for this model is taken as a constant 561 kg / m^3 (Albini, 1985). Using these numbers, the extinction length is calculated to be approximately 5 meters. This shows the extinction length is on the same order as the vertical fuel layer thickness. The application of the extinction parameter will be illustrated in the following chapter.

One should expect, from biological fundamentals, that the extinction length would be on the same order of magnitude as the vertical fuel layer thickness for live, mature vegetation. To illustrate this, the sun can be taken as the radiation source hitting the crown layer of a tree stand. Because the foliage needs the light to photosynthesize, the

foliage will cease to grow when the light is completely absorbed. For this model, this is the location where the stem space layer begins. The fact that it is very dark on the ground beneath a tree stand with a dense canopy validates this reasoning.

CHAPTER 3

SPREAD PROCESS MODELING

Fluid Mechanics of Flames and Fire Plumes

To qualitatively describe the fluid mechanics of flames, the dimensionless heating rate variable Q_d^* is used by Zukoski (Cox, 1995). Q_d^*, also known as the buoyancy flux, has a different form depending upon whether the source of the flame is a one-dimensional or two-dimensional fire. The form discussed by Zukoski is a two-dimensional, circular plate burner with diameter *d*. The remaining terms are the physical parameters that contribute to the properties of the fluid flow. The expression is:

$$Q_d^* = \frac{\dot{Q}_o}{\rho\, T_a c_p (gd)^{\frac{1}{2}} d^2} \tag{26}$$

where *g* is the acceleration of gravity, $\dot{Q}_o$ is the heat release rate of the fuel, and c_p, T_a, and ρ are the specific heat, temperature, and density of ambient gas, respectively.

Another useful idea used in the modeling of flames comes from the entrainment assumption (Morton, Taylor, and Turner 1956). This assumption states that the entrainment of ambient fluid into buoyancy driven flow is proportional to the vertical velocity. The constant of proportionality is known as the entrainment coefficient. The

exact relation for entrainment rate varies with the geometry of the source and has been evaluated by numerous researchers.

Zukoski applies the buoyancy flux relation using the properties of air as the gas the flame is entraining. The flame is divided into three different zones depending on the value of Q_d^*. The first zone is for very small Q_d^* up to a value of 0.1. In this case, the flame is comprised of many small flamelets with the flame lengths of each flamelet much smaller than the burner dimension. This phenomenon is best described in a paper by Heskestad (1991). In the middle zone, Q_d^* falls between 0.1 and 1.0. The flames in this region are no longer many small flamelets but a single short flame. The final zone has Q_d^* greater than 1.0 and is a region where the flame lengths are much larger than the burner diameter. In fires burning in natural fuels, the value of Q_d^* can range in several orders of magnitude and is generally 2.0 and larger. Fortunately, most of the analysis and experimentation has been completed in the region where Q_d^* is greater than 0.1.

The most prominent characteristic of the flames in the region where Q_d^* is greater than 0.1 is the periodic pulsing of the flame. This is due to the rapid reduction of flame diameter near the burner surface, which produces a steady train of puffs. Understanding the pulsations is the key to determining the flame geometry and also plays an important role in fixing the entrainment rate. Photography of flames in this range of Q_d^* show that each puff consists of an axisymmetric, ring-shaped structure that forms next to the burner surface and then rises through the flame. When the value of Q_d^* is greater than 3.0, the

puffs are no longer well defined, but the same behavior can still be identified upon close inspection.

Quantitative measurements through the use of photography are also valuable in the study of flames and fire plumes. The stages of the puffs described in the previous paragraph can be viewed and measured throughout the evolution of its structure. The data obtained from video records serve to support the analytical calculations and also lead to several flame length correlations dependent upon the Q_d^* parameter (Cox, 1995). The relationship for Q_d^* greater than 1.0 is:

$$\frac{H}{d} \propto Q_d^{*\frac{2}{5}} \tag{27}$$

Several different experimentalists have validated this equation.

Using similar derivations and experiments, an algebraic expression can be derived for a line source fire. However, in this case the flame height is proportional to the buoyancy flux to the two-thirds power and b represents the width of the flame base:

$$\frac{H}{b} \propto Q_d^{*\frac{2}{3}} \tag{28}$$

This result is only valid for modeling line source plumes very close to the fire (*i.e.* within a few flame lengths of the fire). Equation (27) must be used to model a line fire far from the source when the geometry of the source is less important. For the radiation driven crown fire model, the flame is modeled as an infinitely long line fire with the region very close to the flame being the area of interest (within about ten extinction lengths).

When the plume is analyzed close to a line source, an important aspect of the fluid mechanics is the power the wind has to push the plume over versus the power the fire has to erect the plume. The model only applies to the case where the plume is able to stand erect in order for radiation to be the driving force of the fire. The case where the wind pushes the flame over is not believed to be steady state and has not been modeled. It is then important to understand when the power of the fire is greater than the power of the wind, defining when the model will apply.

In Brown and Davis (1973), Byram gives relationships for calculating the power of the wind and the power of the fire as follows:

$$P_w = \frac{\rho_{wt} \cdot (v - r)^3}{2g} \tag{29}$$

$$P_f = \frac{I}{c_p \cdot (T_a + 459)} \tag{30}$$

where ρ_{wt} is the weight density of air, $(v - r)$ is the relative wind speed to the fire front, g is the acceleration of gravity, c_p is the specific heat capacity of air, T_a is the ambient temperature, and I is the fire line intensity. This measure of intensity, as always in the study of fire modeling, is in units of power per unit length of fire edge perpendicular to the direction of motion. The calculation for intensity will be shown in equation (42) of the following chapter. The units of the last two equations work out to be power per area.

The ratio of P_f to P_w gives a useful dimensionless quantity to determine whether the wind or the fire is stronger. The power of the wind equation contains the relative velocity raised to the third power, thus if the wind is too great it will push the plume over

and perhaps even blow out the fire. The power of the fire equation contains the line intensity of the fire, thus if the fire has a large value for intensity, the fire will dominate and the flame will stand erect.

However, a question is raised on the physical meaning of the two power equations. In the power of the fire equation, the weight specific heat and temperature terms in the denominator are essentially there to make the units work. The units of weight specific heat multiplied by temperature yield energy divided by force, which reduces to length. An alternative way of obtaining consistent units is to multiply the power of the wind equation by a characteristic height, leaving the power of the fire equation simply as the intensity of the fire. A logical choice for the characteristic height would be the flame height. This is governed by the height at which the mass flow of air is sufficient to burn the mass flow of gaseous pyrolyzate. However, this alteration does not give a better result for the ratio, but only serves to give a more meaningful physical interpretation of the terms.

An alternative way of obtaining essentially the same result is to use Froude scaling in the analysis. The Froude number gives a ratio of wind speed squared to gravity times the height (White, 1994):

$$Fr = \frac{\bar{U}^2}{gH} \tag{31}$$

where $\bar{U}$ is the mean free stream velocity, g is the acceleration of gravity, and H is the characteristic height. This can be applied to a crown fire by visualizing the ability of the wind to overcome the acceleration of gravity and climb over a distance H, with gravity providing the resisting force. The same argument can be made with the wind blowing

against the fire and the plume acting as a barrier of height H. If the wind speed is weak, the plume will cause the wind to blow over the top, and if the wind speed is great enough, the wind will blow the plume over.

It can be shown that the Froude scaling also has the parameter of velocity cubed divided by the intensity (known as Byram's parameter). This is obtained by substituting into equation (31) an expression for the flame height derived from the flame structure model (Albini, 1981):

$$H = \frac{A \cdot I}{\bar{U}} \tag{32}$$

where A is an empirical constant currently taken as 2.65 m^3 / MJ (Albini, 1981). This transforms the Froude number into the following form:

$$Fr = \frac{\bar{U}^3}{gAI} \tag{33}$$

This version of the power of the wind divided by the power of the fire has equal meaning as the version by Byram, but perhaps is more appealing because it was derived from physical arguments.

These ratios determine the relative strength of the wind and fire, and can be calculated using values from actual crown fires. The experimental fires burned in Sharpsand Creek, Ontario, Canada between the years of 1975 to 1981 serve as representative crown fires that are used in testing this model. A complete description of the preburn fuel characteristics, the weather and fire behavior characteristics at the time of the burn, and the total fuel consumed in the fires is given in a paper by Stocks (1987).

This paper gives the values of wind speed and fire intensity necessary to calculate the ratio of the power equations. The density was calculated from the ideal gas law at ambient temperature, and the specific heat was taken from Cengel and Boles (1989) at ambient temperature.

In Table 1, the values for fire intensity and wind speed for the crown fires given in Stocks (1987) are reported. Also, the ratios for both the power of the fire divided by the power of the wind and the reciprocal of the Froude number are given. The ratios indicate that the power of the fire is an order of magnitude greater than the power of the wind. Thus a stable crown fire, once initiated, can exist. This is confirmed from the visual records of the Sharpsand Creek fires that show the fires to have a stable flame structure.

Table 1. Result of the ratio for the power equations.

Fire no.	Intensity (kW/m)	Wind speed (km/h)	Predicted P_f / P_w	Predicted 1/Fr
2	4717	11	18.1	17.1
3	9900	16	12.4	11.7
4	7728	14	14.3	13.6
5	10785	10	55.3	52.1
6	9171	11	35.3	33.4
11a	24274	13	56.6	53.4
11b	40903	21	22.6	21.4
12	17136	14	31.8	30.2
13	15790	15	23.9	22.6
14	25990	16	32.5	30.6

This analysis of the fluid mechanics shows that if the fluid flow close to the fire allows the flame to stand erect, radiation can be identified as the primary heat transfer mechanism. Also, the erect flame will shield the wind causing it to deflect over the top of

the flame. This leaves the area just ahead of the flame with little to no fluid flow and allows the Nusselt number to be taken as that of natural convection. This will be incorporated in the energy balance given in the following section.

The only physical evidence that the wind field is stagnant just ahead of a crown fire was provided by crew leader Wagner Dodge in the fatal Mann Gulch Fire of 1949. Dodge survived by lighting an escape fire just ahead of the advancing crown fire using only a single paper match (a difficult task with strong wind field). His panicked crew refused to follow him into the burned area and all but two perished within 200 yards upslope.

Energy Balance

To mathematically describe the movement of a crown fire, the rate at which heat is transferred to the fuel bed must be modeled. To do this, the complete heat transfer balance is analyzed yielding the temperature distribution of the fuel bed. However, several assumptions are made to simplify the calculations (Albini, 1986). The fire spread is taken as a steady state propagation of an ignition isotherm through a randomly distributed uniform bed of fuel particles. The ignition isotherm is taken to be a diffuse black body radiator. The fuel bed is discretized into a two dimensional grid that is bounded in height by the total height of the fuel, and in length by a finite cold boundary on which the radiation from the free flame and burning zone has little effect on the particle temperature. As was shown before, the particles can be considered thermally thin. The particles are treated as radiometrically black so they do not reflect or scatter radiation.

Radiation impinges on the fuel bed from the free flame, the burning zone, and from other heated fuel. The mathematical representation of the quantity of heat absorbed in the fuel can be analyzed using the radiation transport equation (Albini, 1996). The equation that describes the intensity of the radiation field in the fuel bed is given as:

$$\left(l'\frac{\partial}{\partial x'}+m'\frac{\partial}{\partial y'}+n'\frac{\partial}{\partial z'}\right)\cdot I=-\left(\frac{\beta\sigma}{4}\right)\cdot I+\left(\frac{\beta\sigma}{4\pi}\right)\cdot BT^4 \qquad (34)$$

where (l', m', n') are the direction cosines of the ray path traversed by I, the $\beta\sigma/4$ term was defined previously as the extinction parameter, and T is the local temperature of the fuel particles (Albini, 1996). The net rate of absorption of energy per unit volume can be calculated from equation (34) by taking the negative and integrating over the full solid angle of 4π steradians. The resulting equation is:

$$\dot{Q}''''_{rad}(x,z)=\iint_{4\pi}\left[\frac{\beta\sigma}{4}I-\left(\frac{\beta\sigma}{4\pi}\right)BT^4\right]d\omega' \qquad (35)$$

where $\dot{Q}''''_{rad}$ represents the net rate of heat energy per unit volume being absorbed from the radiation field, ω' is the solid angle, and B is the Stefan-Boltzmann constant. The emissivity is taken as unity because of the black body assumption.

A visual description of how the radiation impinges on the fuel bed is given in Figure 4. In this case, a single ray is shown to travel to the top of the crown layer and then be absorbed while traveling through the fuel. The ray direction is fixed by the direction cosines, l', m', n', and then is integrated over all possible solid angles to obtain the total energy absorbed by the fuel (35).

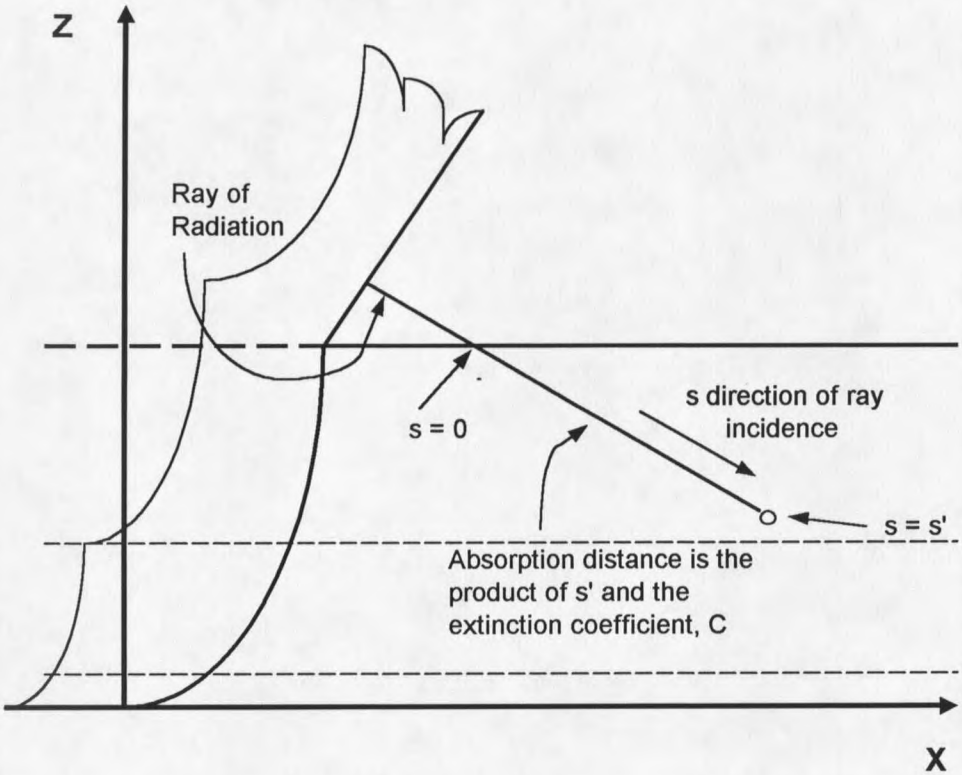

Figure 4. Single radiation ray impinging on fuel bed.

The formulation shown in equation (35) gives the net heating due to radiation, but an additional term pertaining to the cooling of the particles is needed to complete the energy balance. The cooling of the particles by convection due to their elevated temperatures is needed to complete the formulation. The film heat transfer coefficient for the cooling by convection is obtained by an analysis of the Nusselt number associated with the airflow in the fuel bed just ahead of the flaming front. With the above discussion demonstrating the air ahead of the flaming front is essentially stagnant, the convection process can be approximated as natural convection. This assigns the Nusselt number to be

approximately 0.35 (Albini, 1986). The complete formulation of the heat transfer balance including convective cooling is given as follows:

$$\frac{\partial q}{\partial t} = \dot{Q}_{rad}'''(x,z) - h\beta\sigma(T - T_a) \tag{36}$$

where $\frac{\partial q}{\partial t}$ is the complete heat transfer rate per unit volume for the process, T is the surface temperature of the fuel particle, and h is the film heat transfer coefficient. The integration of this equation is an iterative process and, as will be shown in the following chapter, is the inner most iteration in the model code.

Once the heat transfer rate per unit volume in known, the temperature field in the fuel bed can be calculated. The relationship between the net heat absorbed and the temperature is discontinuous due to the moisture content contained in the fuel particle. There are three different regimes where the net heat absorbed changes as a function of temperature (Albini, 1985). The first regime takes the fuel particle to the boiling point. The second regime evaporates the water, and the third regime brings the temperature of the fuel to ignition temperature. These relationships are given as:

$$q_1 = \beta w_o \left(C_f + MC_m\right)\left(T_b - T_a\right) \tag{37}$$

$$q_2 = q_1 + \beta w_o M L_v \tag{38}$$

$$q_i = q_2 + \beta w_o C_f \left(T_i - T_b\right) \tag{39}$$

where C_f and C_m are the specific heats of dry fuel and liquid water respectively, L_v is the latent heat of vaporization of water, T_i, and T_b are the ignition temperature and boiling temperature of the dry fuel particles. A sketch of the three regimes is given in Figure 5.

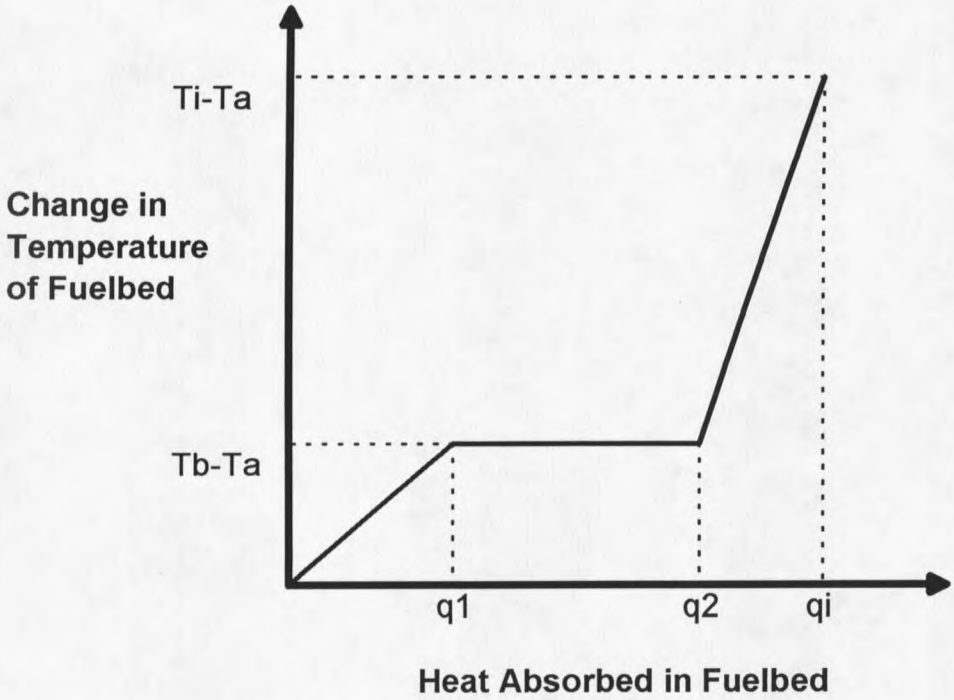

Figure 5. Sketch of $\Delta T_{fuelbed}$ versus the heat absorbed in the fuel bed.

The values the model uses for the calculations are the dimensionless forms of the absorbed heat density, temperature, and intensity source field. These parameters are nondimensionalized to give values that range from zero at ambient conditions to unity at the ignition interface. The spacial variables are also normalized with respect to the fuel bed depth, δ, and then the longitudinal coordinate, x, transformed to fix the interface to the coordinate system:

$$z' = \frac{z}{\delta} \tag{40}$$

$$x' = \frac{(x - St)}{\delta} \tag{41}$$

The height variable, z, ranges from 0 at the base of the fuel bed to unity at the top of the fuel bed. Also, the heat density q is found by integrating equation (36) from time equals minus infinity (x' equals the cold boundary with q known there) to current time, t. The cold boundary location is readily visualized in terms of the moving coordinate x'. The details pertaining to the solution of the radiation transport formulation can be found in Albini (1996).

CHAPTER 4

MODEL STRUCTURE

Four different models have been mentioned thus far in the discussion. These include the fuel consumption model (Call and Albini, in press), the wind velocity profile model (Baughman and Albini, 1980), the flame structure model (Albini, 1981), and the heat transfer model (Albini, 1996). However, before an illustration of how these models relate to one another can be presented, the difference between the rate of spread for a fixed flame geometry, R, and the speed the model predicts using the energy balance, S, must be explained.

The rate of spread corresponding to the flame geometry, R, is used to calculate intensity. This relation is given by:

$$I = H_c \cdot w_c \cdot R \tag{42}$$

where, H_c is the fuel low heat of combustion, w_c is the mass of fuel consumed per unit area, and R is the rate of spread of the fire (Byram, 1959). The flame geometry is calculated for the fire intensity using the flame structure model that was partially presented in equations (14) and (32). The flame geometry consists of the flame height and tilt angle, which are needed for the crown fire model to predict the speed of progress, S. For each value of R, the model will predict a unique value for S. It will be shown below that when

the speed, S, equals the rate, R, the model has converged to a solution at that speed. A diagram of the interaction of the models is given in Figure 6.

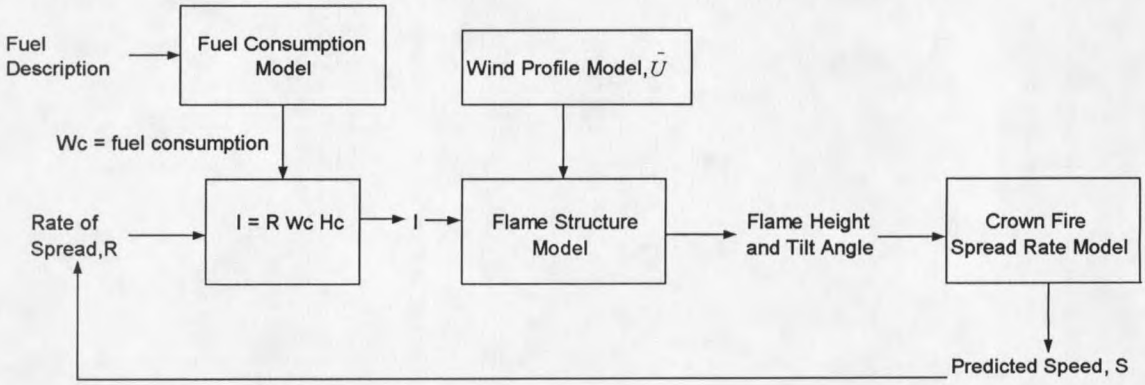

Figure 6. Flow chart showing the different models used in the code.

The specific steps the crown fire model uses to calculate the speed of the fire from the input of the flame height and tilt angle is contained in four levels of iteration as shown in Figure 7. With rate of spread specified initially the intensity and flame geometry is calculated as described above. The interface shape is arbitrarily set to allow the model to begin iterating for the temperature field. With the temperature field known, the interface shape is adjusted to make it an isotherm. The interface is adjusted in small increments and with each adjustment, a new temperature field is calculated. When the interface settles to an isotherm, the speed, S, is changed to move the isotherm toward the ignition temperature. Each time the speed is adjusted, the model will adjust the temperature field and the interface as needed to make the interface an isotherm again. The value for the speed, S, is obtained when the heat absorbed on the interface equals that required for ignition. The final step in the iteration scheme is to compare this speed with the rate used

for the intensity. If these are not equal within a set tolerance, the rate is adjusted and the process starts over. A visual description of the model structure is shown in Figure 7.

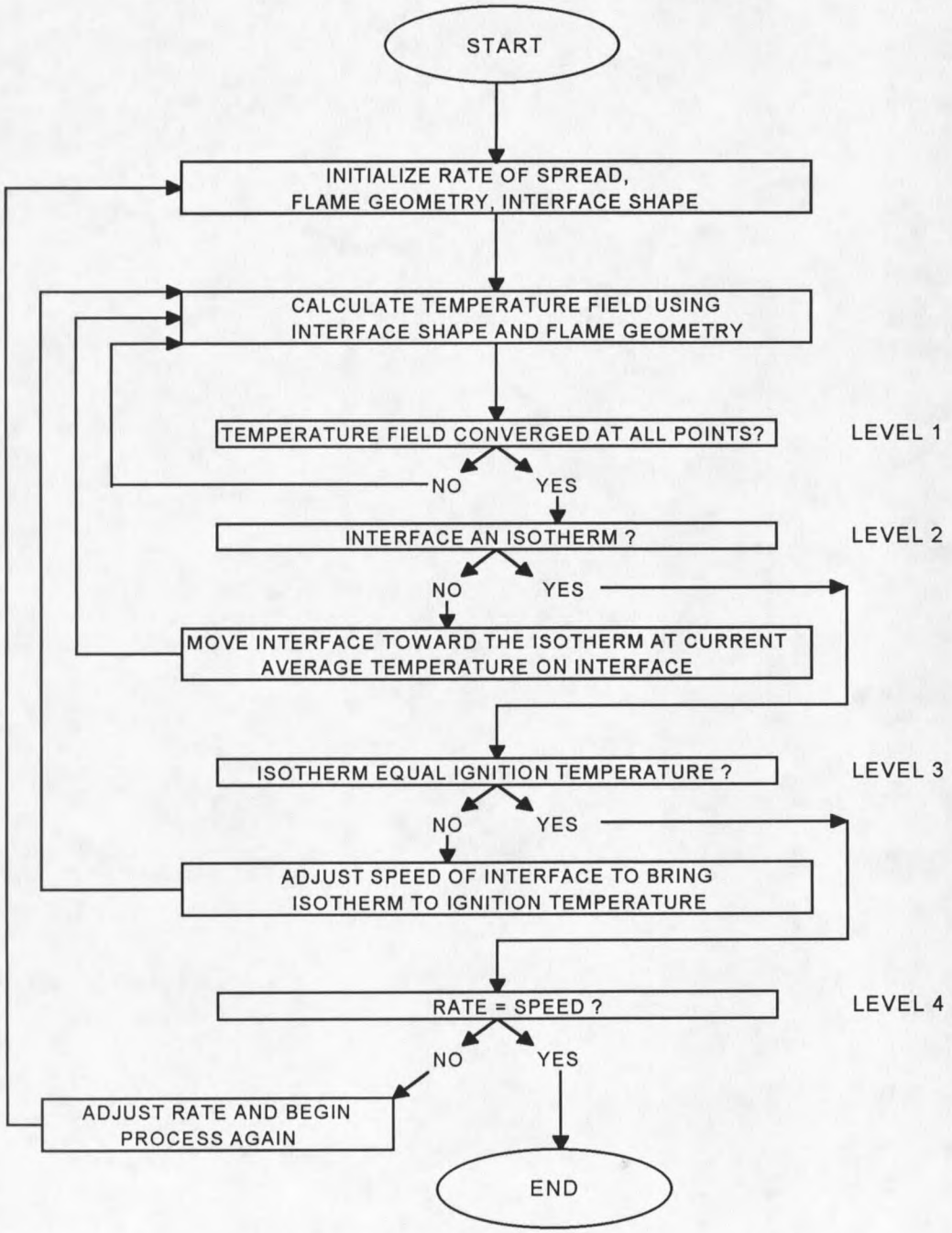

Figure 7. The four levels of iteration performed by the model.

The processor time required to complete the iteration scheme is enormous. Executing the current code on a 386 desktop computer can take several months to calculate a speed with a given intensity. Even on a Pentium 133, it may take several weeks to achieve a complete solution. Thus, an important step in the development of the model is to minimize the number of outer iterations by describing the manner in which the speed predicted by the model behaves with a given input spread rate. If a consistent pattern between predicted fire speed and the spread rate for intensity can be established, a method of accurately predicting the point where the speed equals the spread rate used for intensity can be coded into the model. The method used to correlate the predicted speed with the spread rate used for intensity is given in the next chapter.

CHAPTER 5

MODEL CLOSURE

Sharpsand Creek Experimental Fires

Before the analysis of the closure scheme is presented, a compilation of the results from the Sharpsand Creek experimental fires is given to summarize the performance of the model. For the purpose of simplifying the presentation, much of the data and figures presented are only for Fire 13. Fire 13 was consistently used throughout the project as a representative fire because of the complete visual record taken at the time of the fire. The records include slides and video that can be readily compared to the computer generated data and predictions.

In Table 2, the relevant fuel characteristics are given. Excluded from the table are the oven dry fuel density, the mineral ash percentage, and the heat of combustion because these values were presumed to be constant for all size classes of each layer. The value for the oven dry density is taken as 561 kg/m^3, the mineral ash content is 5 percent, and the heat of combustion is a constant 17,500 kJ/kg (Stocks, 1987). The moisture values came either from Stocks (1995) or the U.S. Forest Service's fuel moisture charts (Burgan, Cohen, Deeming 1977). The details of how these resources were used to obtain the moisture contents are given in Call and Albini (in press).

Table 2. Fuel description for Sharpsand Creek Fire 13.

Fuel layer / size class (cm)	fuel loading (kg/m^2)	specific heat (kJ/kgK)	sigma 4/D (m^{-1})	moisture content (%)
Surface layer				
Litter	0.308	1.50	6450	12.5
< 0.99	0.062	1.50	800	10.2
1.0-3.0	0.230	1.50	200	11.0
3.0-7.0	0.092	1.50	80.0	17.0
> 7.0	1.290	1.50	53.3	17.0
understory	0.088	1.80	6450	209
dead boles	0.031	1.50	241	11.0
live boles	0.260	1.50	77.8	70.0
Stem Space layer				
dead boles	0.031	1.50	241	11.0
live boles	0.260	1.50	77.8	70.0
dead trees	0.182	1.50	800	11.0
Crown layer				
foliage	0.977	1.80	6450	209
limbwood	0.572	1.50	800	11.0
branches	0.410	1.50	800	70.0

Table 3 gives the results of the single equivalent fuel characteristic algorithm. The table includes the oven dry density, but since the ash content and the heat of combustion remain constant before and after the routine at 5 percent and 17,500 kJ/kg respectively, they are excluded from the table. The density of the fuel decreases because only the fuel that is consumed by the flame is included in the equivalent fuel description. Thus, the density shown in Table 3 is unrealistic, but is intended to represent a one-component equivalent fuel bed. The fuel description and equivalent fuel characteristics for all the Sharpsand Creek fires are given in Appendix A.

Table 3. The equivalent fuel characteristics for Sharpsand Creek Fire 13.

Fuel Layer	fuel loading (kg/m^3)	oven dry density (kg/m^3)	specific heat (kJ/kgK)	Sigma 4/D (m^{-1})	moisture content(%)
Surface layer	0.6511	171.5	1.541	593.3	42.4
Stem space layer	0.9012	111.3	1.500	123.3	36.7
Crown layer	1.7380	497.6	1.669	3534	74.8

The fire behavior results of the model for each crown fire at Sharpsand Creek is shown in Table 4. The table gives the calculated flame height and compares the predicted rates of spread and intensity with the observed rates of spread and intensity for each fire. The differences in the spread rates translate into the differences in the intensity due to their interdependence (see equation 42). The predicted and observed spread rates for Fire 13 are the same because this fire was used to gauge the radiometric temperature of the burning zone. The radiometric temperature of the burning zone at which the two spread rates conformed was found to be approximately 1050 Kelvin. Note the systematic error in spread rate prediction: The model underestimates the speeds of fires that spread faster than the calibration fire (0.270 m/s) and overestimates the speeds of fires slower than this one. The reasons for the errors in the model are currently being explored. It is believed that the radiometric burning zone temperature changes as a function of intensity. This would allow the fires with higher intensity to burn faster, and the fires with lower intensity to burn slower. Research is currently being planned to obtain hard data for the radiometric burning zone temperature as a function of intensity.

Table 4. Predicted and Observed fire behavior quantities for the Sharpsand Creek Fires.

Fire No.	Flame Height (m)	Rate of Spread Calculated (m/s)	Rate of Spread Observed (m/s)	Intensity Predicted (kW/m)	Intensity Observed (kW/m)
2	7.30	0.276	0.179	13930	4714
3	4.73	0.301	0.281	11690	9900
4	6.06	0.289	0.238	13990	7728
5	8.86	0.315	0.244	16230	10785
6	8.75	0.316	0.243	17580	9171
11a	7.35	0.300	0.489	16610	24274
11b	5.44	0.331	0.824	18290	40903
12	5.75	0.286	0.336	13090	17136
13	5.98	0.270	0.270	14770	15790
14	5.36	0.281	0.455	13700	25990

The interface shape for each Sharpsand Creek fire was calculated and plotted. Figure 8 shows three different isotherms located in the fuel bed of Fire 13. The first isotherm is the ignition interface shape. The two other isotherms are the locations in the fuel bed ahead of the flame front where the fuel has reached the point of desiccation and the surface on which it has just reached boiling point. The drastic discontinuities are located at the top of the surface and stem space layers. This is a result of the programming and is not necessarily the true shape of the interface. Methods of correcting this phenomenon are currently being investigated. The isotherm plots for the fires are shown in Appendix B.

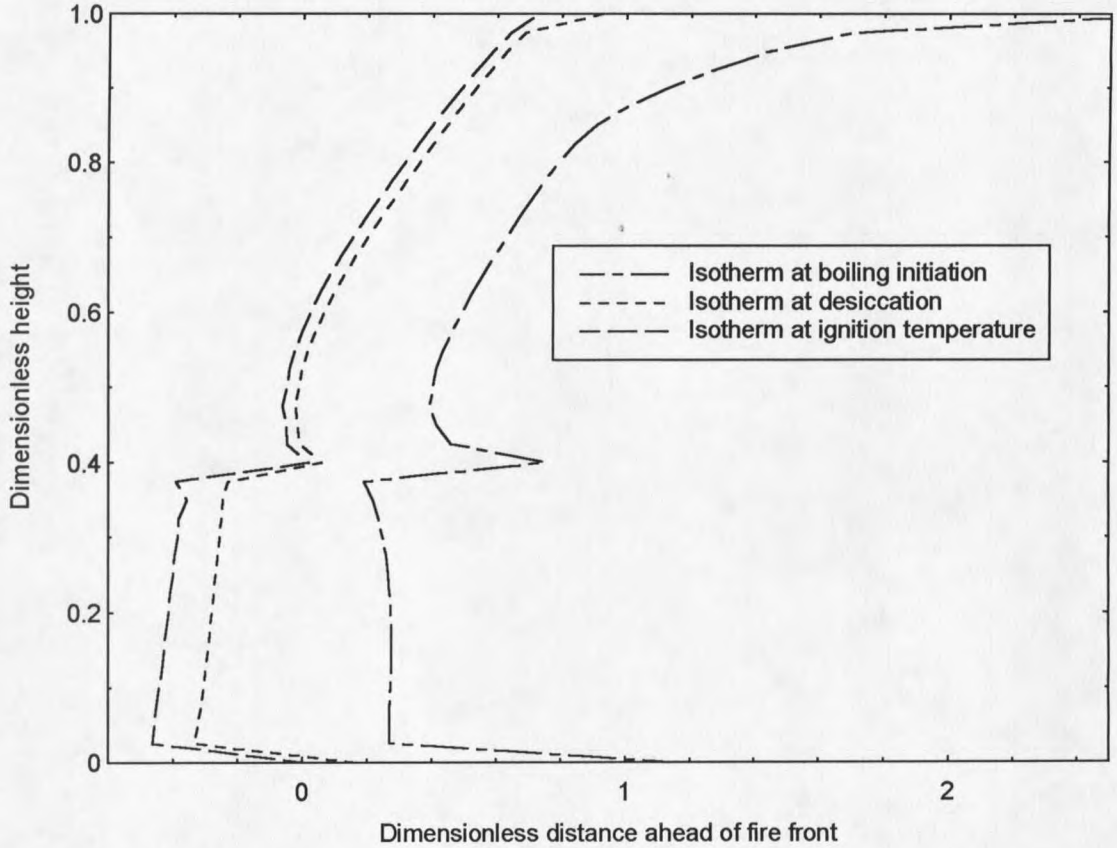

Figure 8. Ignition interface with isotherms at the desiccation and boiling temperatures.

Closure Scheme

To find a suitable closure scheme that allows the model to converge to a solution quickly, a correspondence between spread rate used to calculate intensity and the speed the model predicts can be developed. Experimental runs of the model were executed for each crown fire using a wide range of input spread rates. The speed the model predicted was recorded along with the input spread rate, and plots were created for each fire using each speed and rate pair as a data point. The resulting plot for Fire 13 is shown in Figure 9 and is typical of the results for other fires. The data plots a line with a correlation

coefficient of 1.00. Also on this figure is a 45-degree line that represents possible solutions of rate equaling the speed. The intersection of this line with the linear curve fit is the overall predicted speed of the fire. It can be seen that the model will predict a unique overall speed for each fire. For each fire, the pattern of speed versus rate was linear as is shown with Fire 13.

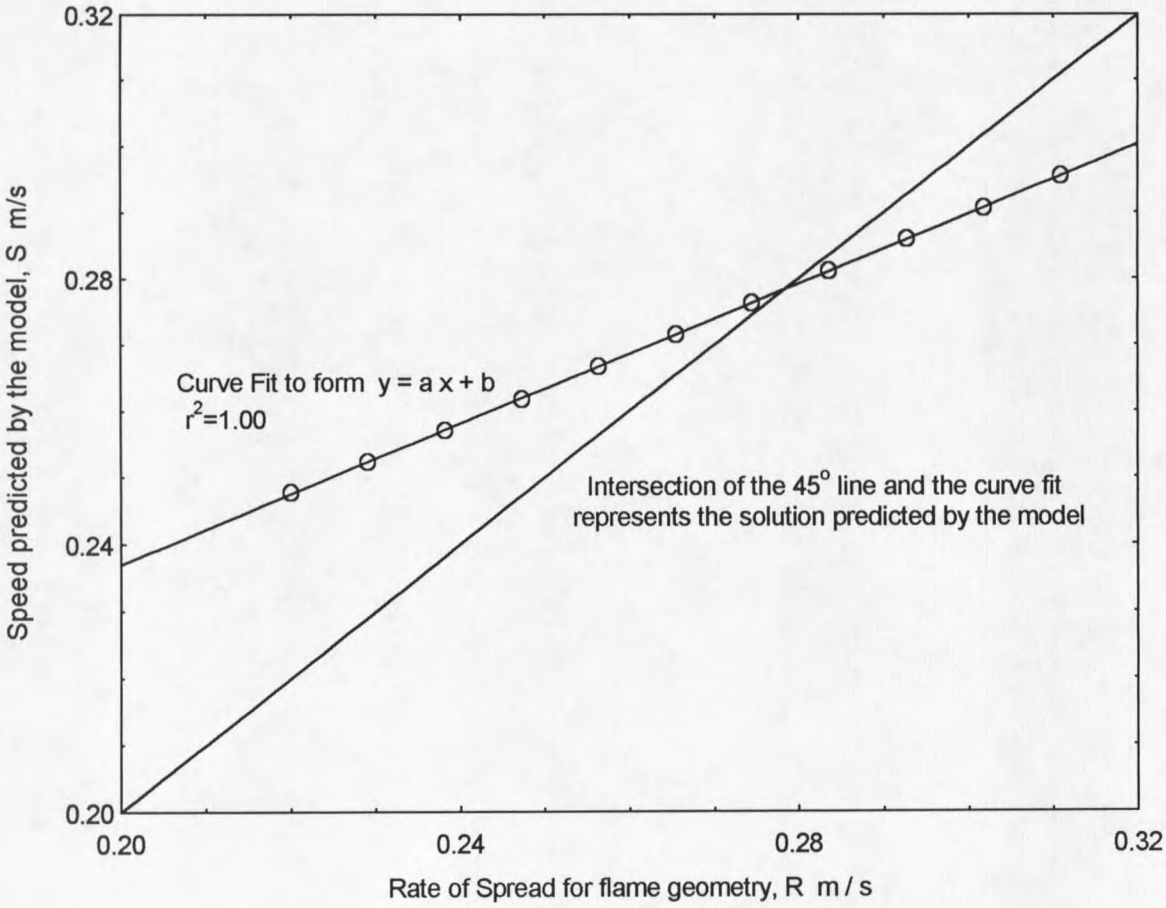

Figure 9. Curve fit for spread rate prediction for Fire 13.

The plot of speed versus rate for Fire 13 has an r^2 value of 1.00. However, this is not always the case as can be seen in Figure 10. The data points appear to be scattered, but actually two different sets of data each plot a straight line above and below the

regression line. The phenomenon is explained by the error tolerance parameter used to determine convergence being too large. However, due to the nature of the numerical scheme, a smaller error tolerance may not always achieve convergence. Figure 10 demonstrates that with the scattered distribution, the best fit is still linear. The remaining plots of each of the other crown fires are shown in Appendix C.

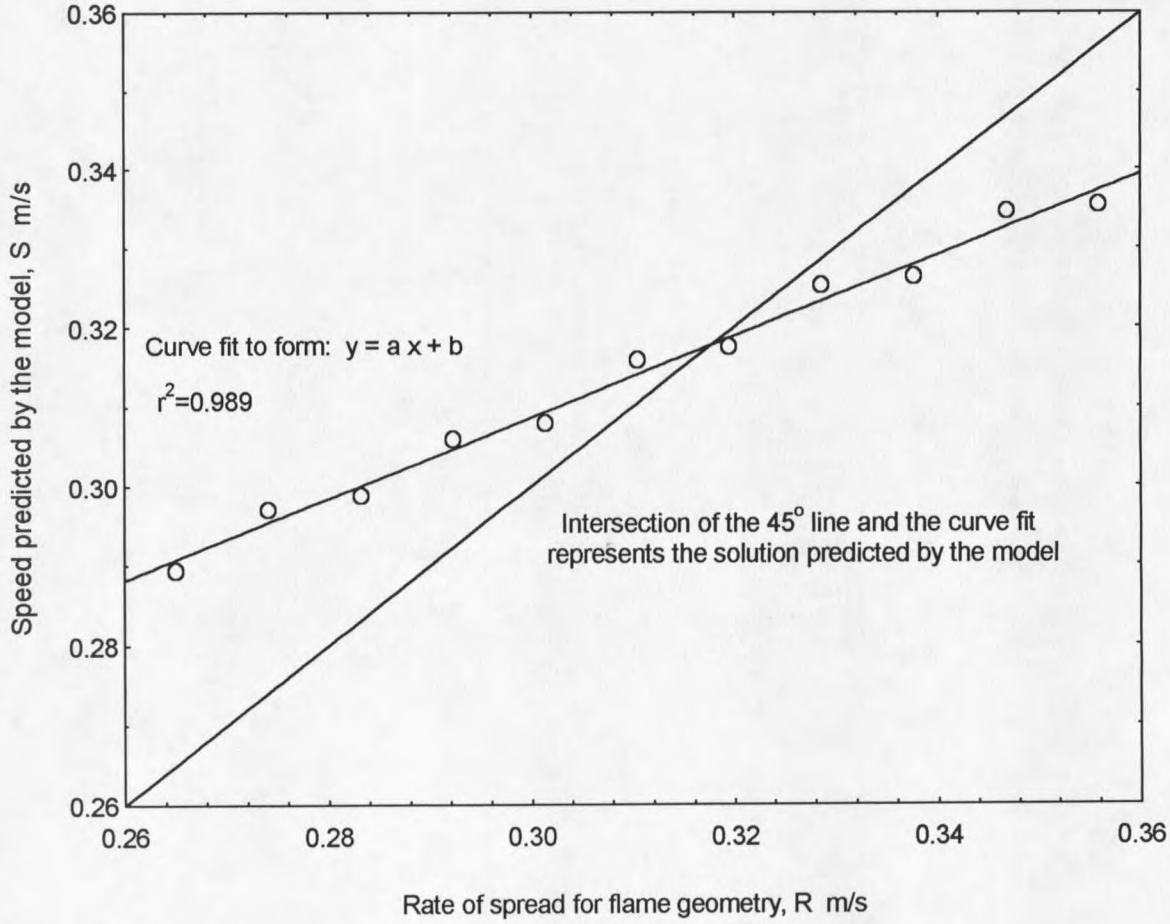

Figure 10. Curve fit for spread rate prediction for Fire 5.

With the relationship between speed and rate established as linear, the model code was changed to accurately predict the solution. The logic the model uses to arrive at the predicted spread rate is shown on Figure 11. To describe the line of speed versus rate, two

points are needed. Once the equation of the speed versus rate line is known, it can be equated to the 45-degree line to calculate the solution. Each of these steps is described in detail in the following paragraph.

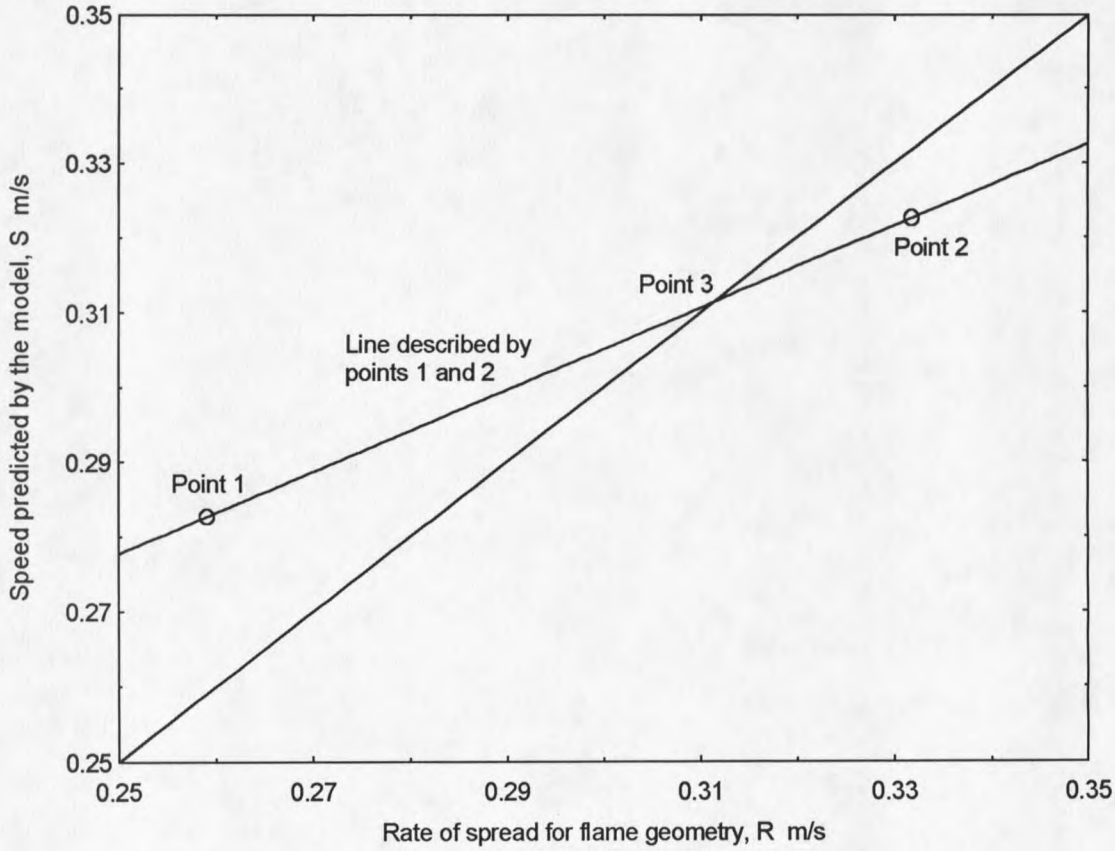

Figure 11. Logic the model uses to converge to a solution.

The model accepts an initial guess for the rate and predicts the speed for that particular rate (point 1). The next value for the rate is calculated by arbitrarily assuming the slope of the line describing speed versus rate to be 0.5. This gives the rate used to calculate the speed at point 2. Once the speed corresponding to the second rate is determined, the true slope of the line is calculated (shown on graph on Figure 11). The third rate is taken as the intersection of the calculated line and the 45-degree line. The

model then performs a third calculation to confirm the speed equals the rate (point 3). If the speed and rate are not equal to a given tolerance, the model will calculate a new line using points 2 and 3 and again equate this to the 45-degree line. A fourth trial is then performed to confirm the rate equals the speed. This process of taking the final two points and calculating a new slope can be repeated indefinitely until the rate equals the speed. However, if the closure scheme performs as expected, only a total of three outer iterations will be needed.

The effectiveness of the closure scheme is still being determined. Approximately 10 trials using the Sharpsand Creek experimental fires have been executed using the new scheme, and each converged in three outer iterations. At this point all the data available from the experimental fires has been exhausted and further testing will be needed to prove the closure scheme will converge in three trials each time.

With the implementation of the closure scheme, the processor time needed to produce a solution has been dramatically reduced. It was mentioned earlier that it might take several weeks to find a solution on a Pentium 133 starting from an arbitrary spread rate used to calculate intensity. The total time to achieve a solution has been reduced to under a single day, and sometimes as fast as two hours. Although the calculation of a fourth point or fifth point has not been needed, the time required to complete the solution if additional points were calculated would, in all likelihood, be under a single day. Thus, the closure scheme makes a vast improvement on the usability of the model.

Previously, the relationship between speed and rate was thought to behave like a square root function or a similar polynomial. This could be true if the range were

increased to give a larger spread of data. However, the range shown is representative of actual crown fires. For this range the linear fit appears to work very well, so there is not a need to develop a more complicated fit.

An important characteristic of the data is that the slope of the speed versus rate line must be less than one. As can be seen in Figures 9 and 10, if the slope were greater than one, the model would become unstable causing the closure scheme to diverge. Table 5 shows the slopes of each Sharpsand Creek experimental crown fire to be less than one. The table also shows the correlation coefficient calculated for plots of each fire.

Table 5. Slopes and correlation coefficients of the speed versus rate lines for the Sharpsand Creek fires.

Fire no.	slope	correlation coefficient, r^2
2	0.512	0.992
3	0.217	0.998
4	0.450	1.000
5	0.512	0.989
6	0.573	0.990
11a	0.547	0.996
11b	0.559	0.993
12	0.352	0.999
13	0.529	1.000
14	0.396	1.000

Future Work

Planned for the summer of 1997 is another set of experimental fires to be burned in the Northwest Territories of Canada. For each of the planned burns, an extensive inventory of the fuel characteristics has been made. The fuel has been classified into size

categories and analyzed for loading and mass density. These data will be fed into the fuel consumption model and a single equivalent size class will be created for each layer in the fuel bed. The model can then be executed to give a predicted spread rate for the experimental fire. The closure scheme will then be tested further to ensure the model will close in three outer iterations. The post-burn fuel characteristics will be analyzed to determine the exact amount of fuel consumed by the flame. This will be compared to the fuel consumption predicted by the model.

An important parameter in the calculation of the energy balance is the effective radiometric temperature of the burning zone, which will be measured in the Northwest Territories experimental fires. This parameter thus far has been estimated from limited data taken from laboratory fires. However, a radiometer invented by Dr. Bret Butler of the Intermountain Research Station, Missoula, MT will be able to accurately measure the radiometric temperature inside the burning zone. These data will hopefully relate the intensity of the fire to the radiometric temperature, which can then be incorporated into the model.

REFERENCES

REFERENCES CITED

Albini, Frank A., 1981: "A Model for the Wind-Blown Flame from a Line Fire", *Combustion and Flame*, **43**: 155-174.

Albini, Frank A., 1984: "Wildland Fires", *American Scientist*, **72**: 590-597.

Albini, Frank A., 1986: "Wildland Fire Spread by Radiation-A Model Including Fuel Cooling by Natural Convection", *Combustion Science and Technology*, **45:** 101-103.

Albini, Frank A., Stocks, Brian J., 1986: "Predicted and Observed Rates of Spread of Crown Fires in Immature Jack Pine", *Combustion Science and Technology*, **48:** 65-76.

Albini, Frank A., 1993: "Dynamics and Modeling of Vegetation Fires: Observations", Chapter 3, pp. 39-52, in Crutzen, P. J., Goldammer, J. G., editors, "Fire in the Environment: The Ecological, Atmospheric, and Climatic Importance of Vegetation Fires", John Wiley and Sons, Chichester, England, 400 pages.

Albini, Frank A., 1995: "Modeling Ignition and Burning Rate of Large Woody Natural Fuels", *International Journal of Wildland Fire*, **5** (2) 81-91.

Albini, Frank A., 1996: "Iterative Solution of the Radiation Transport Equations Governing Spread of Fire in Wildland Fuel", *Fizika Goreniya i Vzryva*, **32** (5): 71-82.

Baughman R. G., Albini, F. A., 1980: "Estimating Midflame Windspeeds", Proc. Sixth Conference on Fire and Forestry Meteorology, R. E. Martin et al., editors, Washington, DC: *Society of American Foresters*, pp. 88-92.

Brown, Arthur A., Davis, Kenneth P., 1973: "Forest Fire: Use and Control", 2nd edn., McGraw-Hill, New York, pp. 208-210.

Burgan, R. E., Cohen, J. D., and Deeming, J. E., 1977: Manually calculating fire-danger ratings -- 1978 National Fire Danger Rating System. USDA Forest Service General Technical Report INT-40, 51 pp. Intermountain Research Station, Ogden UT.

Byram, G. M., 1959: "Combustion of Forest Fuels. Forest Fire: Control and Use.", Davis, K. P., editor, McGraw-Hill, New York, pp. 61-89.

Cox, Geoffrey, 1995: "Combustion Fundamentals of Fire", Academic Press, London, England, Ch. 1-3,7.

Call, Patrick, Albini, Frank, 1996: "Aerial and Surface Fuel Consumption in Crown Fires", *International Journal of Wildland Fire*, in-press.

Cengel, Yunus A., Boles, Michael A., 1989: "Thermodynamics: An Engineering Approach", McGraw-Hill, New York, p. 820.

Drysdale, Dougal, 1985: "An Introduction to Fire Dynamics", John Wiley and Sons, Chichester, England, Ch 1-4.

Glassman, Irvin, 1977: "Combustion", Academic Press, New York, Ch 4.

Incropera, Frank P., DeWitt, David P. 1990: "Fundamentals of Heat and Mass Transfer", 3rd edn., John Wiley and Sons, New York, p. 230.

Heskestad, Gunnar, 1991: "A Reduced-Scale Mass Fire Experiment", *Combustion and Flame,* **83**: (3-4) 61-73.

Morton, B. R., Taylor, G. I., Turner, J.S., 1956: "Turbulent gravitational convection from maintained and instantaneous sources", *Proc. Royal Soc.* **A234:** 1-23.

Spalding, D. B., 1976: *Combustion Science and Technology,* **13**: 3.

Stocks, B. J., 1987: "Fire behavior in immature jack pine", *Can. J. For. Res.* **17**: 80-86.

Stocks, B. J., 1995: Moisture measurements for Sharpsand Creek experimental fires. Personal communication, 6 December 1995.

Stockstad, D. S., 1975: "Spontaneous and piloted ignition of pine needles", USDA Forest Service Research Note INT-204, Intermountain Research Station, Ogden UT, 12 pp.

Van Wagner, C. E., 1977: "Conditions for the start and spread of crown fire", *Can. J. For. Res.* **7**: 23-34.

White, Frank M., 1994: "Fluid Mechanics", 3rd edn., McGraw-Hill, New York, p. 268.

APPENDICES

APPENDIX A

FUEL DATA AND EQUIVALENT FUEL CHARACTERISTICS

Table A1. Fuel description for Sharpsand Creek Fire 2.

Fuel layer / size class (cm)	fuel loading (kg/m^2)	specific heat (kJ/kgK)	sigma 4/D (m^{-1})	moisture content (%)
Surface layer				
Litter	0.219	1.50	6450	11.0
< 0.99	0.072	1.50	800	10.7
1.0-3.0	0.047	1.50	200	11.0
3.0-7.0	0.078	1.50	80.0	17.0
> 7.0	1.370	1.50	53.3	17.0
understory	0.088	1.80	6450	184
dead boles	0.031	1.50	241	11.0
live boles	0.260	1.50	77.8	70.0
Stem Space layer				
dead boles	0.031	1.50	241	11.0
live boles	0.260	1.50	77.8	70.0
dead trees	0.142	1.50	800	8.51
Crown layer				
foliage	0.939	1.80	6450	184
limbwood	0.512	1.50	800	8.51
branches	0.410	1.50	800	70.0

Table A2. The equivalent fuel characteristics for Sharpsand Creek Fire 2.

Fuel Layer	fuel loading (kg/m^2)	oven dry density (kg/m^3)	specific heat (kJ/kgK)	Sigma 4/D (m^{-1})	moisture content(%)
Surface layer	0.5353	150.1	1.549	547.3	45.0
Stem space layer	0.8612	107.3	1.500	117.3	37.4
Crown layer	1.640	494.2	1.672	3563	73.1

Table A3. Fuel description for Sharpsand Creek Fire 3.

Fuel layer / size class (cm)	fuel loading (kg/m^2)	specific heat (kJ/kgK)	sigma 4/D (m^{-1})	moisture content (%)
Surface layer				
Litter	0.240	1.50	6450	11.0
< 0.99	0.100	1.50	800	10.7
1.0-3.0	0.089	1.50	200	11.0
3.0-7.0	0.000	1.50	80.0	17.0
> 7.0	0.238	1.50	53.3	17.0
understory	0.088	1.80	6450	184
dead boles	0.031	1.50	241	11.0
live boles	0.260	1.50	77.8	70.0
Stem Space layer				
dead boles	0.031	1.50	241	11.0
live boles	0.260	1.50	77.8	70.0
dead trees	0.073	1.50	800	8.51
Crown layer				
foliage	0.622	1.80	6450	209
limbwood	0.339	1.50	800	8.51
branches	0.410	1.50	800	70.0

Table A4. The equivalent fuel characteristics for Sharpsand Creek Fire 3.

Fuel Layer	fuel loading (kg/m^2)	oven dry density (kg/m^3)	specific heat (kJ/kgK)	Sigma 4/D (m^{-1})	moisture content(%)
Surface layer	0.3902	252.8	1.568	1262	54.5
Stem space layer	0.7922	100.2	1.500	106.7	40.0
Crown layer	1.150	470.4	1.662	3244	73.0

Table A5. Fuel description for Sharpsand Creek Fire 4.

Fuel layer / size class (cm)	fuel loading (kg/m^2)	specific heat (kJ/kgK)	sigma 4/D (m^{-1})	moisture content (%)
Surface layer				
Litter	0.238	1.50	6450	15.0
< 0.99	0.070	1.50	800	19.7
1.0-3.0	0.158	1.50	200	15.0
3.0-7.0	0.090	1.50	80.0	19.0
> 7.0	1.120	1.50	53.3	19.0
understory	0.088	1.80	6450	262
dead boles	0.031	1.50	241	15.0
live boles	0.260	1.50	77.8	70.0
Stem Space layer				
dead boles	0.031	1.50	241	11.0
live boles	0.260	1.50	77.8	70.0
dead trees	0.313	1.50	800	10.4
Crown layer				
foliage	0.718	1.80	6450	263
limbwood	0.414	1.50	800	10.4
branches	0.410	1.50	800	70.0

Table A6. The equivalent fuel characteristics for Sharpsand Creek Fire 4.

Fuel Layer	fuel loading (kg/m^2)	oven dry density (kg/m^3)	specific heat (kJ/kgK)	Sigma 4/D (m^{-1})	moisture content(%)
Surface layer	0.5480	163.9	1.548	604.1	42.4
Stem space layer	1.0320	123.9	1.500	142.3	36.7
Crown layer	1.3210	480.4	1.663	3324	74.8

Table A7. Fuel description for Sharpsand Creek Fire 5.

Fuel layer / size class (cm)	fuel loading (kg/m^2)	specific heat (kJ/kgK)	sigma 4/D (m^{-1})	moisture content (%)
Surface layer				
Litter	0.251	1.50	6450	9.00
< 0.99	0.101	1.50	800	9.10
1.0-3.0	0.113	1.50	200	9.00
3.0-7.0	0.079	1.50	80.0	15.0
> 7.0	2.090	1.50	53.3	15.0
understory	0.088	1.80	6450	226
dead boles	0.031	1.50	241	9.00
live boles	0.260	1.50	77.8	70.0
Stem Space layer				
dead boles	0.031	1.50	241	11.0
live boles	0.260	1.50	77.8	70.0
dead trees	0.183	1.50	800	8.75
Crown layer				
foliage	0.782	1.80	6450	226
limbwood	0.466	1.50	800	8.75
branches	0.410	1.50	800	70.0

Table A8. The equivalent fuel characteristics for Sharpsand Creek Fire 5.

Fuel Layer	fuel loading (kg/m^2)	oven dry density (kg/m^3)	specific heat (kJ/kgK)	Sigma 4/D (m^{-1})	moisture content(%)
Surface layer	0.7556	150.1	1.535	432.4	42.4
Stem space layer	0.9022	111.4	1.500	123.4	36.7
Crown layer	1.4370	486.1	1.663	3366	74.8

Table A9. Fuel description for Sharpsand Creek Fire 6.

Fuel layer / size class (cm)	fuel loading (kg/m^2)	specific heat (kJ/kgK)	sigma 4/D (m^{-1})	moisture content (%)
Surface layer				
Litter	0.236	1.50	6450	9.00
< 0.99	0.078	1.50	800	9.10
1.0-3.0	0.125	1.50	200	9.00
3.0-7.0	0.093	1.50	80.0	15.0
> 7.0	3.830	1.50	53.3	15.0
understory	0.088	1.80	6450	226
dead boles	0.031	1.50	241	9.00
live boles	0.260	1.50	77.8	70.0
Stem Space layer				
dead boles	0.031	1.50	241	11.0
live boles	0.260	1.50	77.8	70.0
dead trees	0.133	1.50	800	8.75
Crown layer				
foliage	0.836	1.80	6450	226
limbwood	0.430	1.50	800	8.75
branches	0.410	1.50	800	70.0

Table A10. The equivalent fuel characteristics for Sharpsand Creek Fire 6.

Fuel Layer	fuel loading (kg/m^2)	oven dry density (kg/m^3)	specific heat (kJ/kgK)	Sigma 4/D (m^{-1})	moisture content(%)
Surface layer	1.0410	128.0	1.525	279.3	32.8
Stem space layer	0.8522	106.4	1.500	115.9	37.8
Crown layer	1.4550	486.9	1.672	3520	76.6

Table A11. Fuel description for Sharpsand Creek Fire 11.

Fuel layer / size class (cm)	fuel loading (kg/m^2)	specific heat (kJ/kgK)	sigma 4/D (m^{-1})	moisture content (%)
Surface layer				
Litter	0.253	1.50	6450	10.9
< 0.99	0.040	1.50	800	9.90
1.0-3.0	0.084	1.50	200	10.0
3.0-7.0	0.034	1.50	80.0	13.0
> 7.0	3.630	1.50	53.3	13.0
understory	0.088	1.80	6450	240
dead boles	0.031	1.50	241	10.0
live boles	0.260	1.50	77.8	70.0
Stem Space layer				
dead boles	0.031	1.50	241	11.0
live boles	0.260	1.50	77.8	70.0
dead trees	0.131	1.50	800	12.0
Crown layer				
foliage	0.888	1.80	6450	240
limbwood	0.473	1.50	800	12.0
branches	0.410	1.50	800	70.0

Table A12. The equivalent fuel characteristics for Sharpsand Creek Fire 11a and 11b.

Fuel Layer	fuel loading (kg/m^2)	oven dry density (kg/m^3)	specific heat (kJ/kgK)	Sigma 4/D (m^{-1})	moisture content(%)
Surface layer	0.9655	128.0	1.527	295.2	34.7
Stem space layer	0.8502	106.2	1.500	115.6	38.3
Crown layer	1.514	489.4	1.676	3597	77.9

Table A13. Fuel description for Sharpsand Creek Fire 12.

Fuel layer / size class (cm)	fuel loading (kg/m^2)	specific heat (kJ/kgK)	sigma 4/D (m^{-1})	moisture content (%)
Surface layer				
Litter	0.281	1.50	6450	12.5
< 0.99	0.081	1.50	800	10.2
1.0-3.0	0.167	1.50	200	11.0
3.0-7.0	0.079	1.50	80.0	17.0
> 7.0	1.380	1.50	53.3	17.0
understory	0.088	1.80	6450	209
dead boles	0.031	1.50	241	11.0
live boles	0.260	1.50	77.8	70.0
Stem Space layer				
dead boles	0.031	1.50	241	11.0
live boles	0.260	1.50	77.8	70.0
dead trees	0.176	1.50	800	11.0
Crown layer				
foliage	0.646	1.80	6450	209
limbwood	0.389	1.50	800	11.0
branches	0.410	1.50	800	70.0

Table A14. The equivalent fuel characteristics for Sharpsand Creek Fire 12.

Fuel Layer	fuel loading (kg/m^2)	oven dry density (kg/m^3)	specific heat (kJ/kgK)	Sigma 4/D (m^{-1})	moisture content(%)
Surface layer	0.6360	165.5	1.542	569.0	42.4
Stem space layer	0.8952	110.7	1.500	122.4	36.7
Crown layer	1.224	475.0	1.658	3212	74.8

Table A15. Fuel description for Sharpsand Creek Fire 13.

Fuel layer / size class (cm)	fuel loading (kg/m^2)	specific heat (kJ/kgK)	sigma 4/D (m^{-1})	moisture content (%)
Surface layer				
Litter	0.308	1.50	6450	125
< 0.99	0.062	1.50	800	10.2
1.0-3.0	0.230	1.50	200	11.0
3.0-7.0	0.092	1.50	80.0	17.0
> 7.0	1.290	1.50	53.3	17.0
understory	0.088	1.80	6450	209
dead boles	0.031	1.50	241	11.0
live boles	0.260	1.50	77.8	70.0
Stem Space layer				
dead boles	0.031	1.50	241	11.0
live boles	0.260	1.50	77.8	70.0
dead trees	0.182	1.50	800	11.0
Crown layer				
foliage	0.977	1.80	6450	209
limbwood	0.572	1.50	800	11.0
branches	0.410	1.50	800	70.0

Table A16. The equivalent fuel characteristics for Sharpsand Creek Fire 13.

Fuel Layer	fuel loading (kg/m^2)	oven dry density (kg/m^3)	specific heat (kJ/kgK)	Sigma 4/D (m^{-1})	moisture content(%)
Surface layer	0.6511	171.5	1.541	593.3	42.4
Stem space layer	0.9012	111.3	1.500	123.3	36.7
Crown layer	1.7380	497.6	1.669	3534	74.8

Table A17. Fuel description for Sharpsand Creek Fire 14.

Fuel layer / size class (cm)	fuel loading (kg/m^2)	specific heat (kJ/kgK)	sigma 4/D (m^{-1})	moisture content (%)
Surface layer				
Litter	0.282	1.50	6450	14.4
< 0.99	0.099	1.50	800	11.9
1.0-3.0	0.270	1.50	200	11.0
3.0-7.0	0.106	1.50	80.0	16.0
> 7.0	1.760	1.50	53.3	16.0
understory	0.088	1.80	6450	240
dead boles	0.031	1.50	241	11.0
live boles	0.260	1.50	77.8	70.0
Stem Space layer				
dead boles	0.031	1.50	241	11.0
live boles	0.260	1.50	77.8	70.0
dead trees	0.151	1.50	800	11.0
Crown layer				
foliage	0.682	1.80	6450	240
limbwood	0.398	1.50	800	11.0
branches	0.410	1.50	800	70.0

Table A18. The equivalent fuel characteristics for Sharpsand Creek Fire 14.

Fuel Layer	fuel loading (kg/m^2)	oven dry density (kg/m^3)	specific heat (kJ/kgK)	Sigma 4/D (m^{-1})	moisture content(%)
Surface layer	0.7951	166.2	1.533	478.9	40.7
Stem space layer	0.8702	108.2	1.500	118.6	37.6
Crown layer	1.2690	477.6	1.661	3276	75.1

APPENDIX B

FUEL BED ISOTHERMS

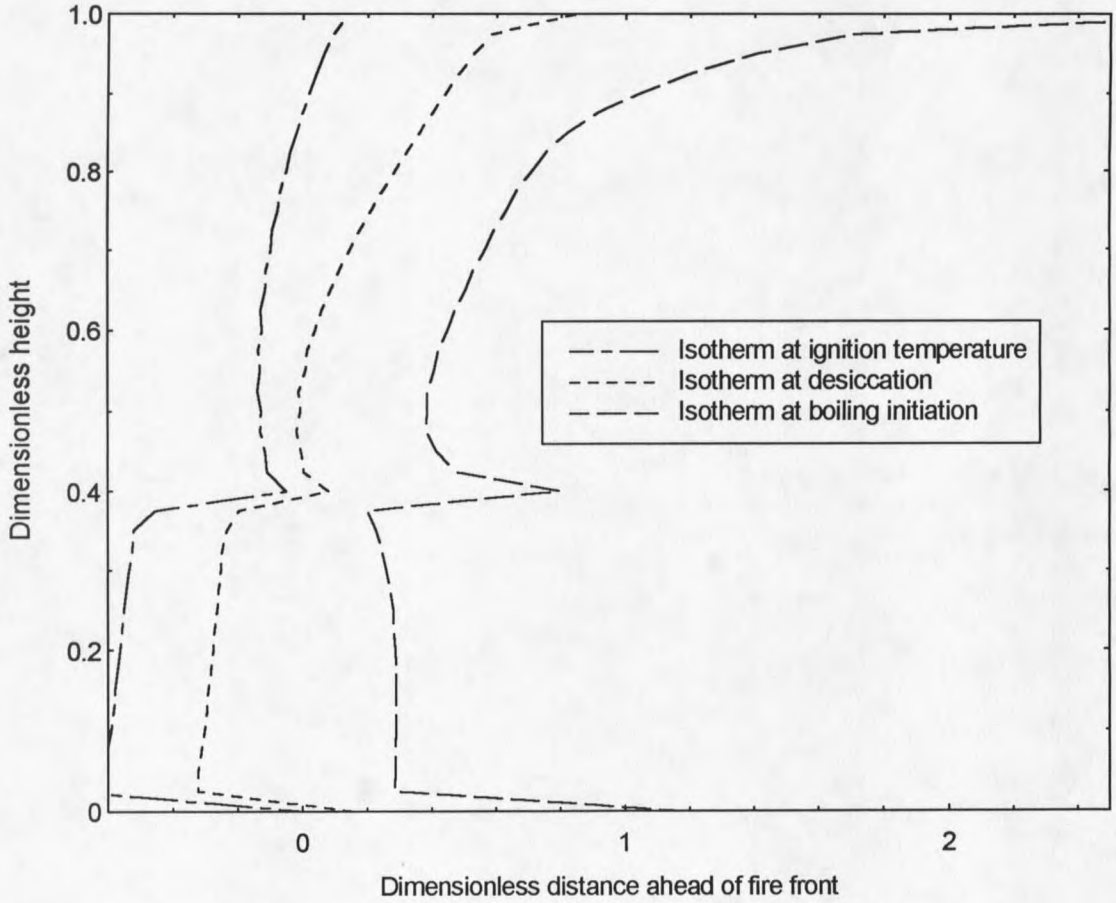

Figure B1. Ignition interface with isotherms at the desiccation and boiling temperatures for Fire 2.

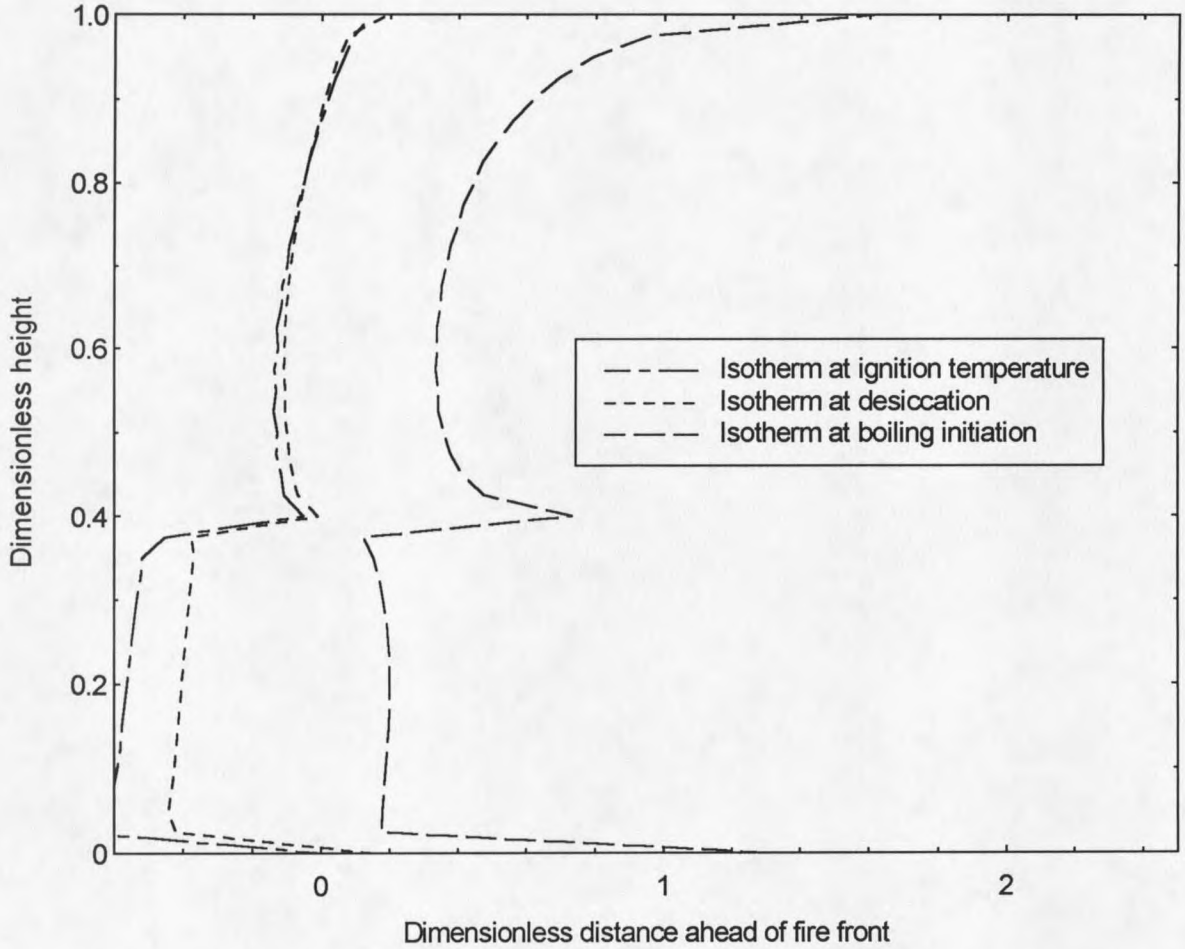

Figure B2. Ignition interface with isotherms at the desiccation and boiling temperatures for Fire 3.

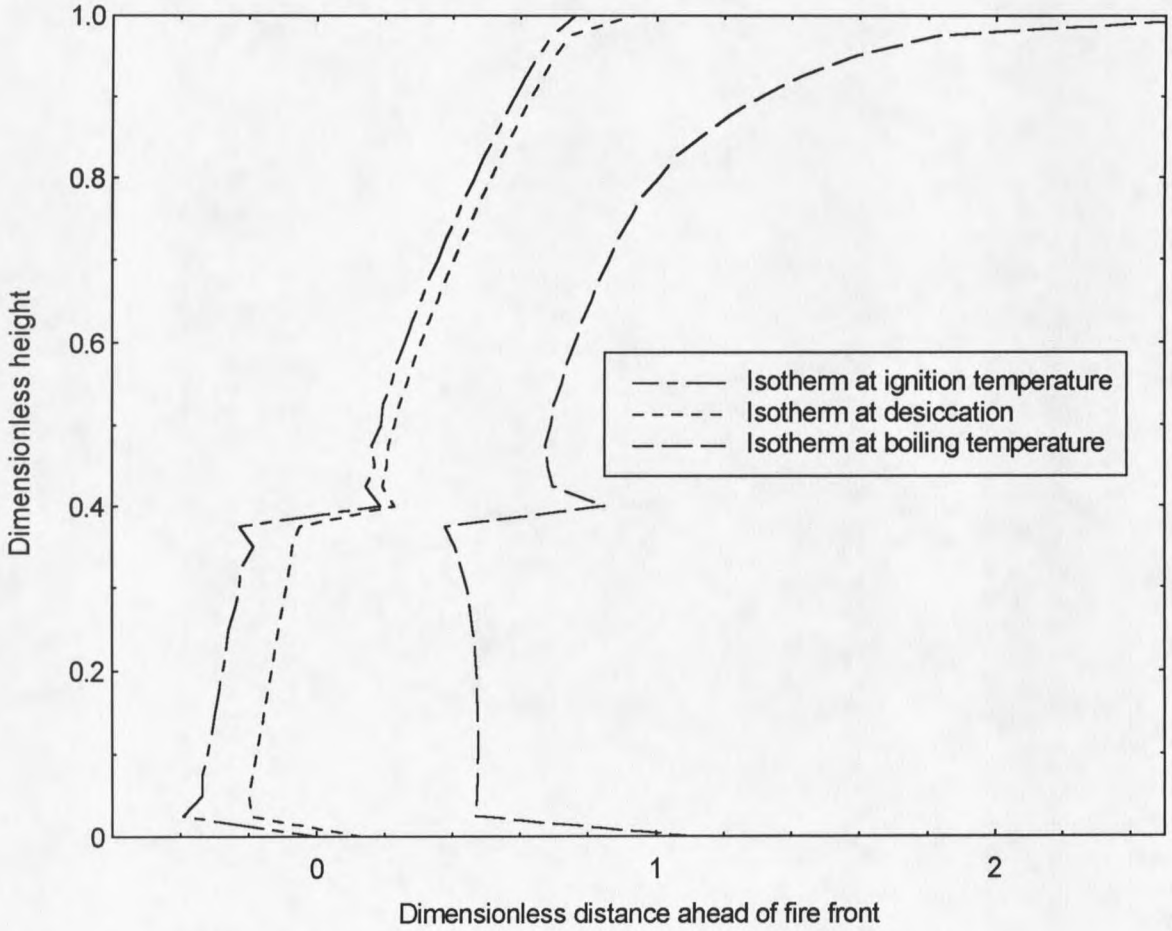

Figure B3. Ignition interface with isotherms at the desiccation and boiling temperatures for Fire 4.

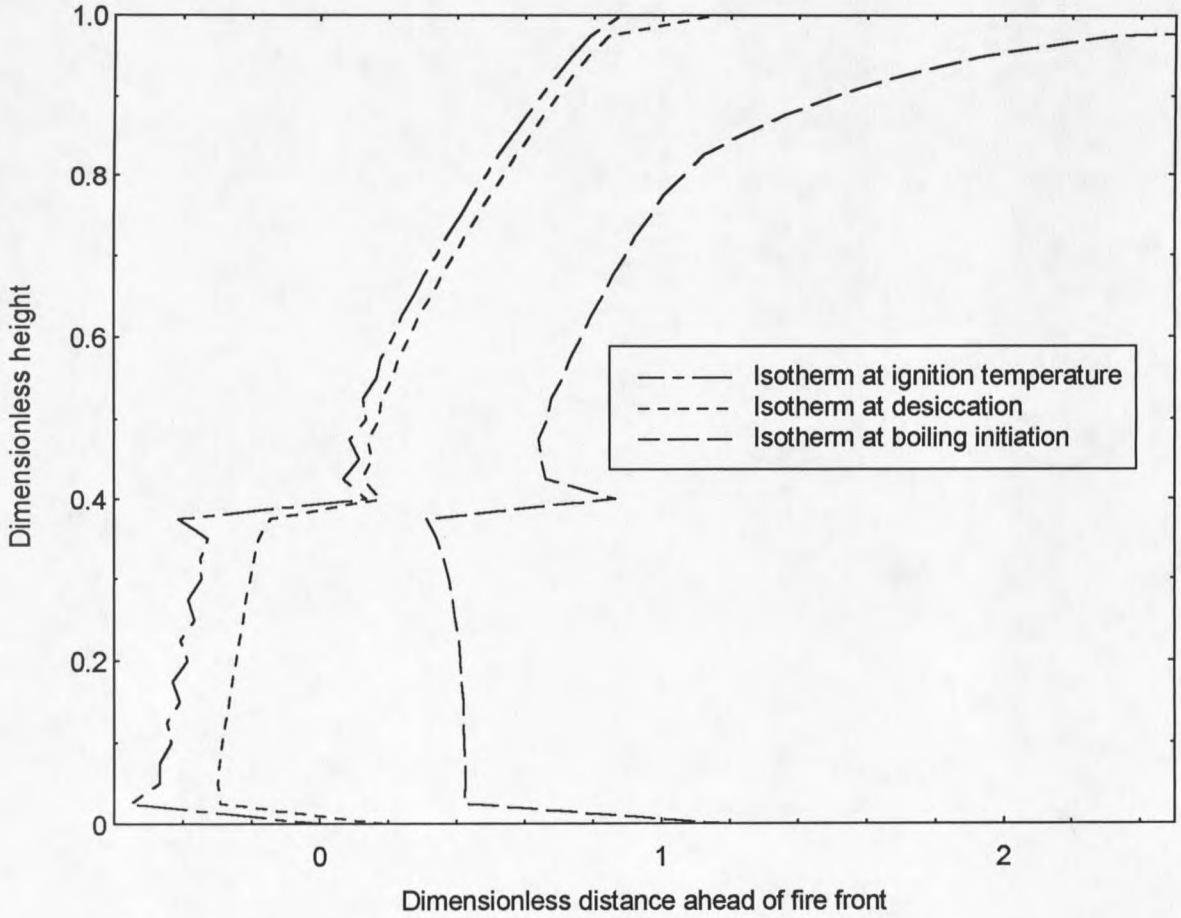

Figure B4. Ignition interface with isotherms at the desiccation and boiling temperatures for Fire 5.

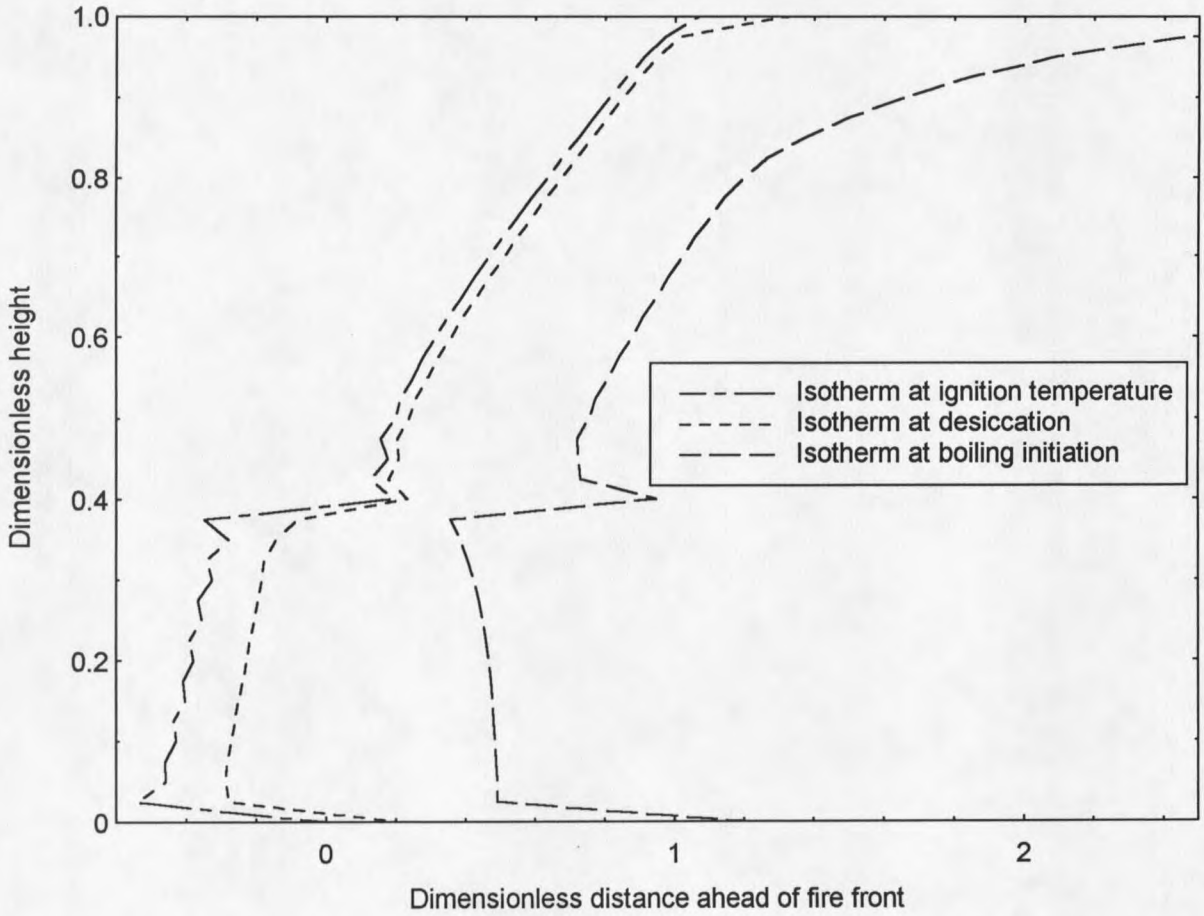

Figure B5. Ignition interface with isotherms at the desiccation and boiling temperatures for Fire 6.

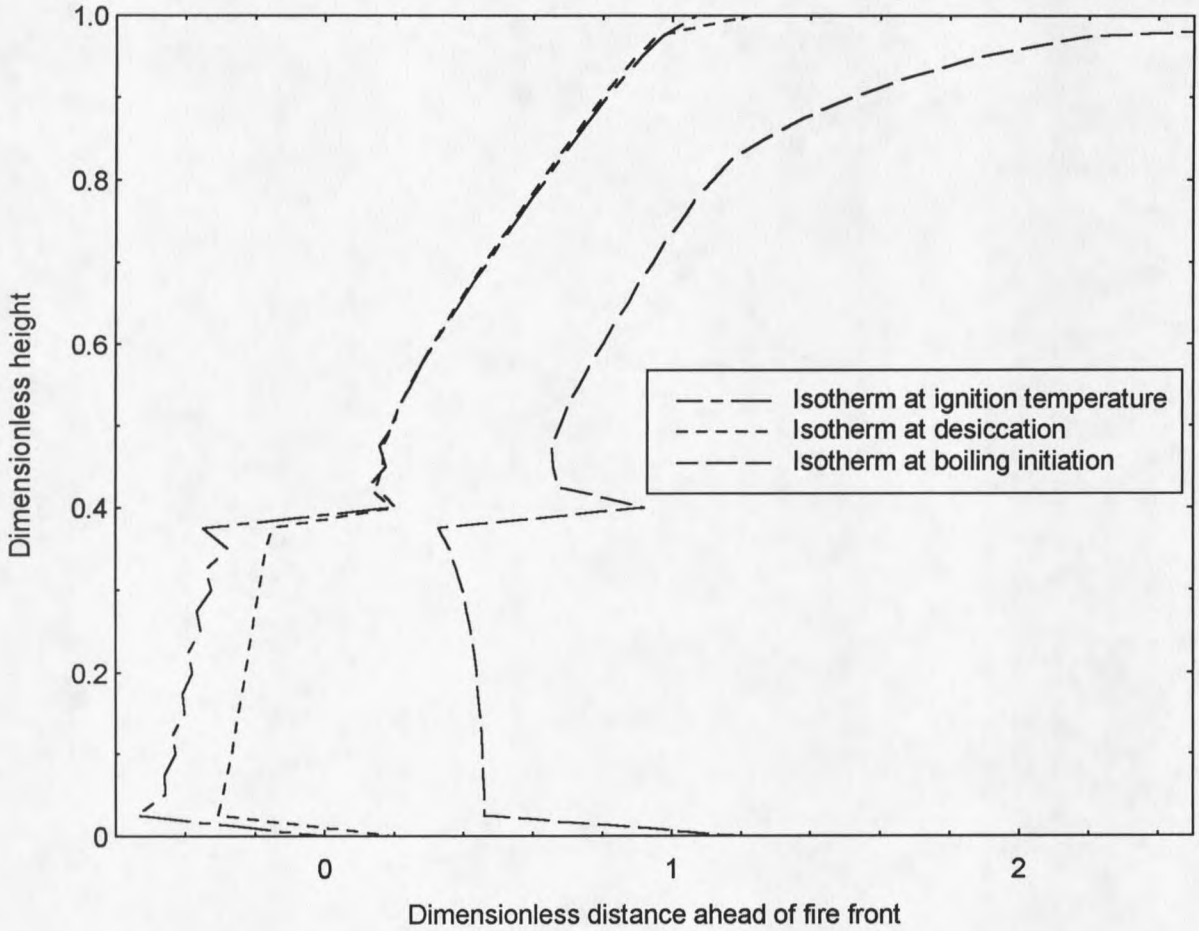

Figure B6. Ignition interface with isotherms at the desiccation and boiling temperatures for Fire 11a.

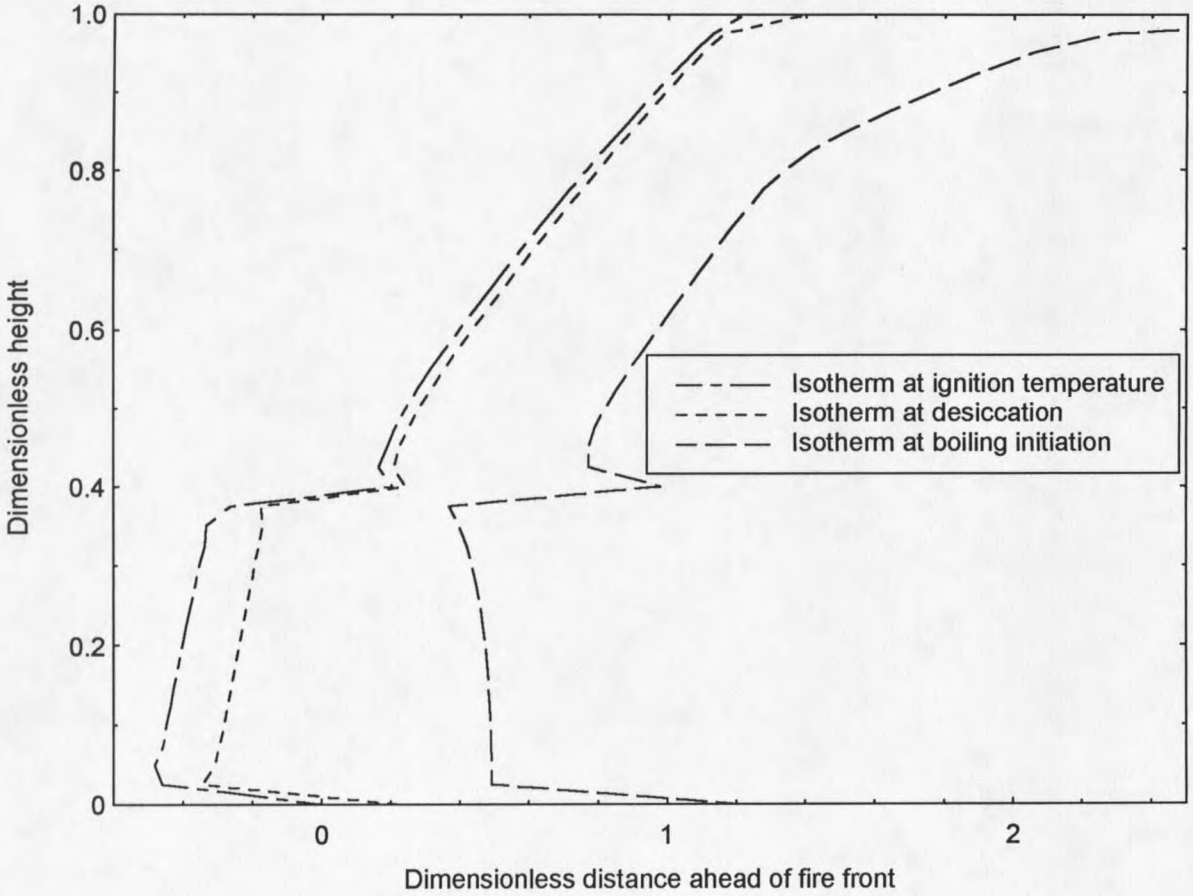

Figure B7. Ignition interface with isotherms at the desiccation and boiling temperatures for Fire 11b.

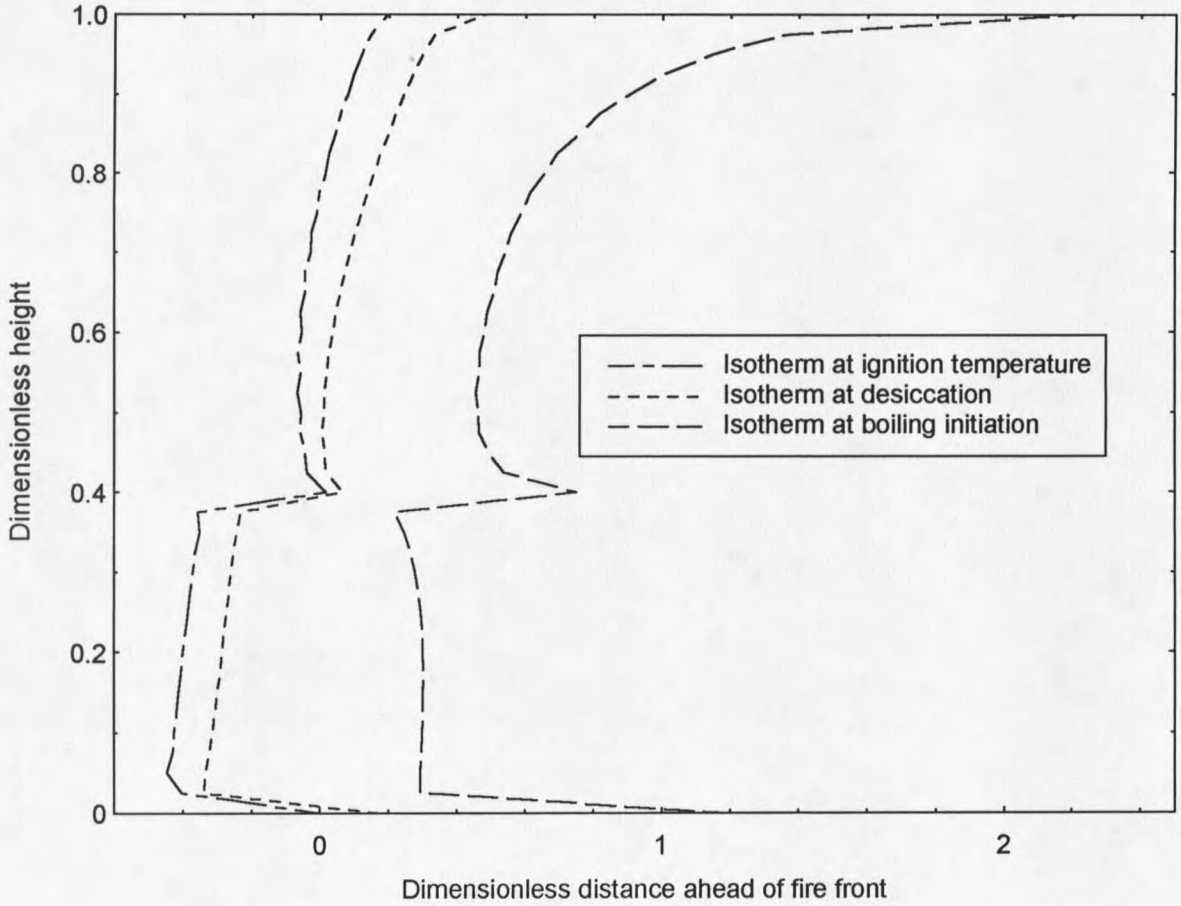

Figure B8. Ignition interface with isotherms at the desiccation and boiling temperatures for Fire 12.

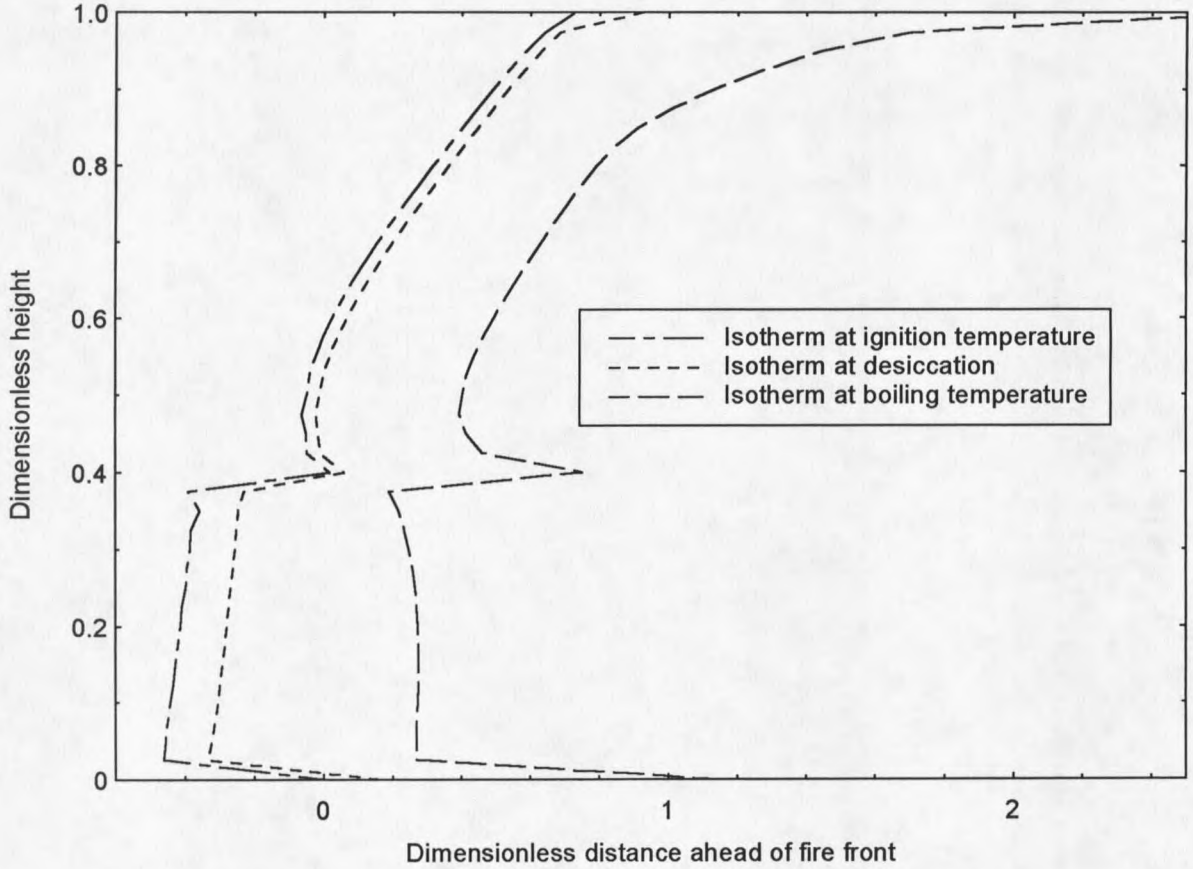

Figure B9. Ignition interface with isotherms at the desiccation and boiling temperatures for Fire 13.

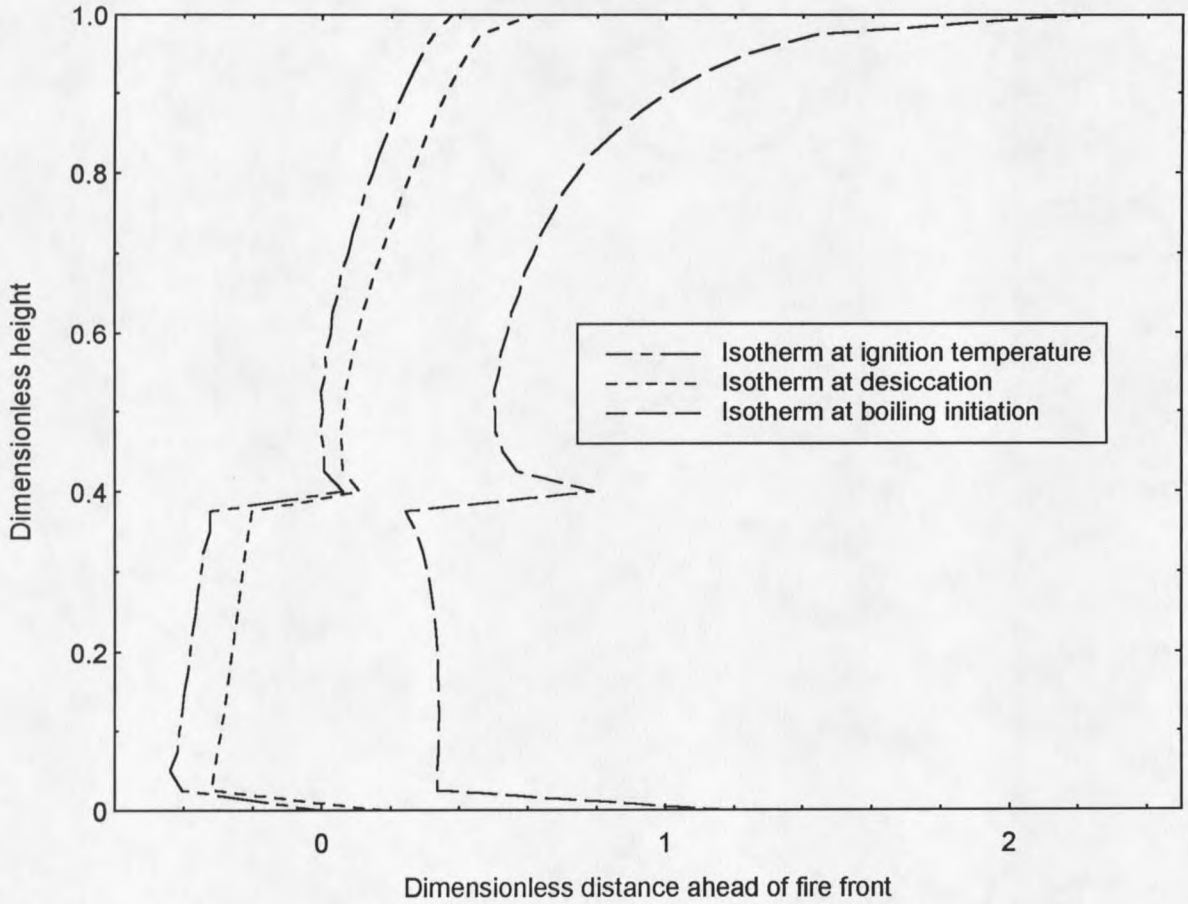

Figure B10. Ignition interface with isotherms at the desiccation and boiling temperatures for Fire 14.

APPENDIX C

CURVE FIT FOR SPREAD RATE PREDICTION

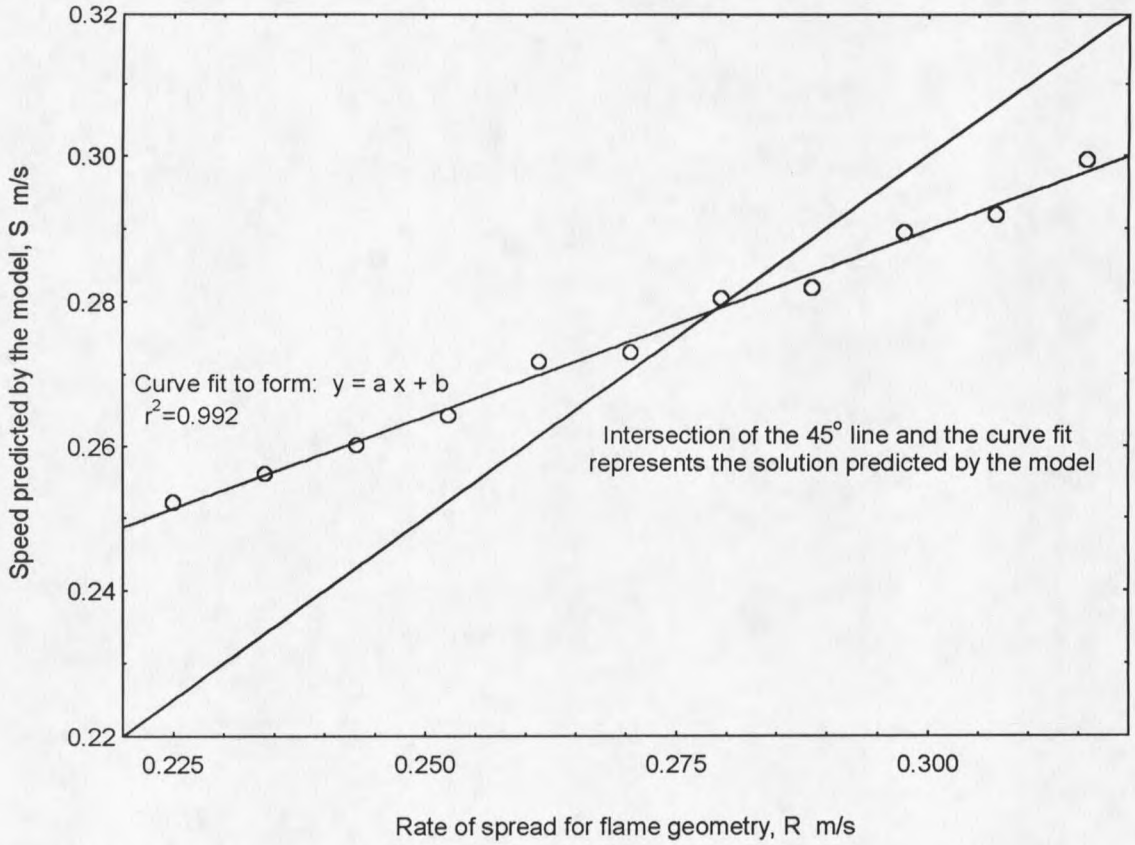

Figure C1. Curve fit for spread rate prediction for Fire 2.

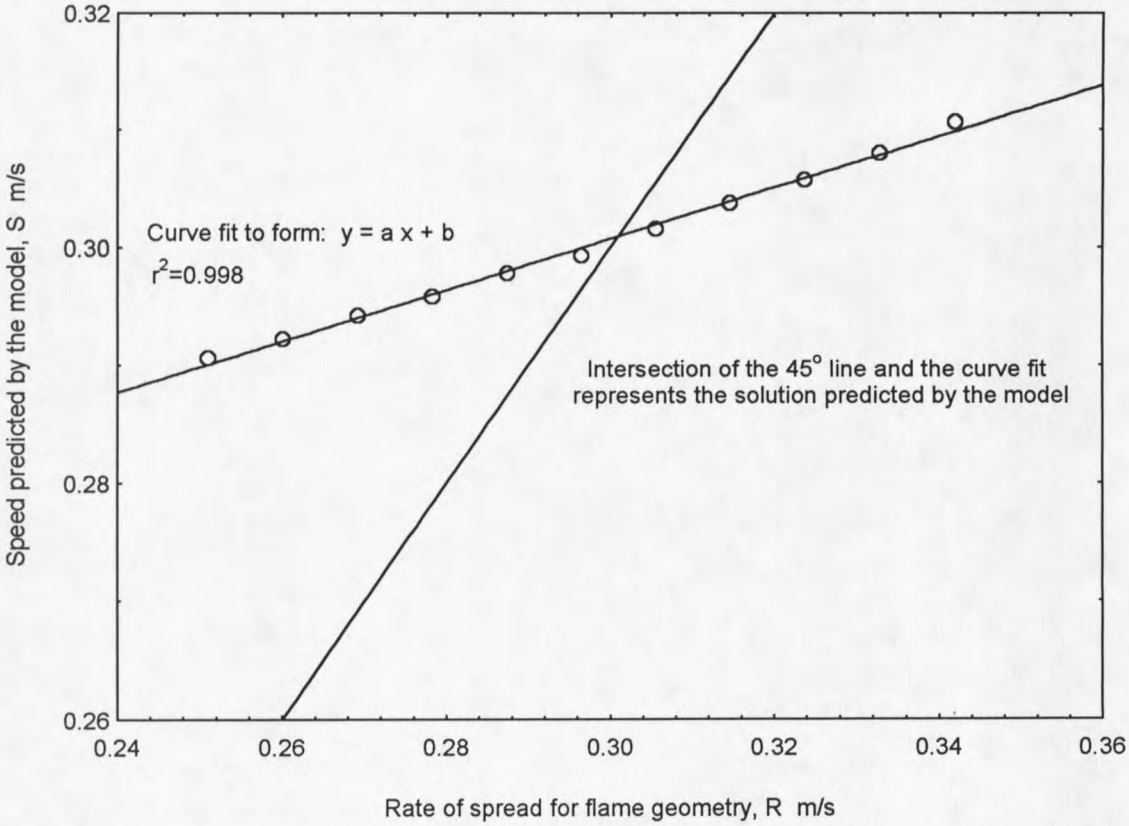

Figure C2. Curve fit for spread rate prediction for Fire 3.

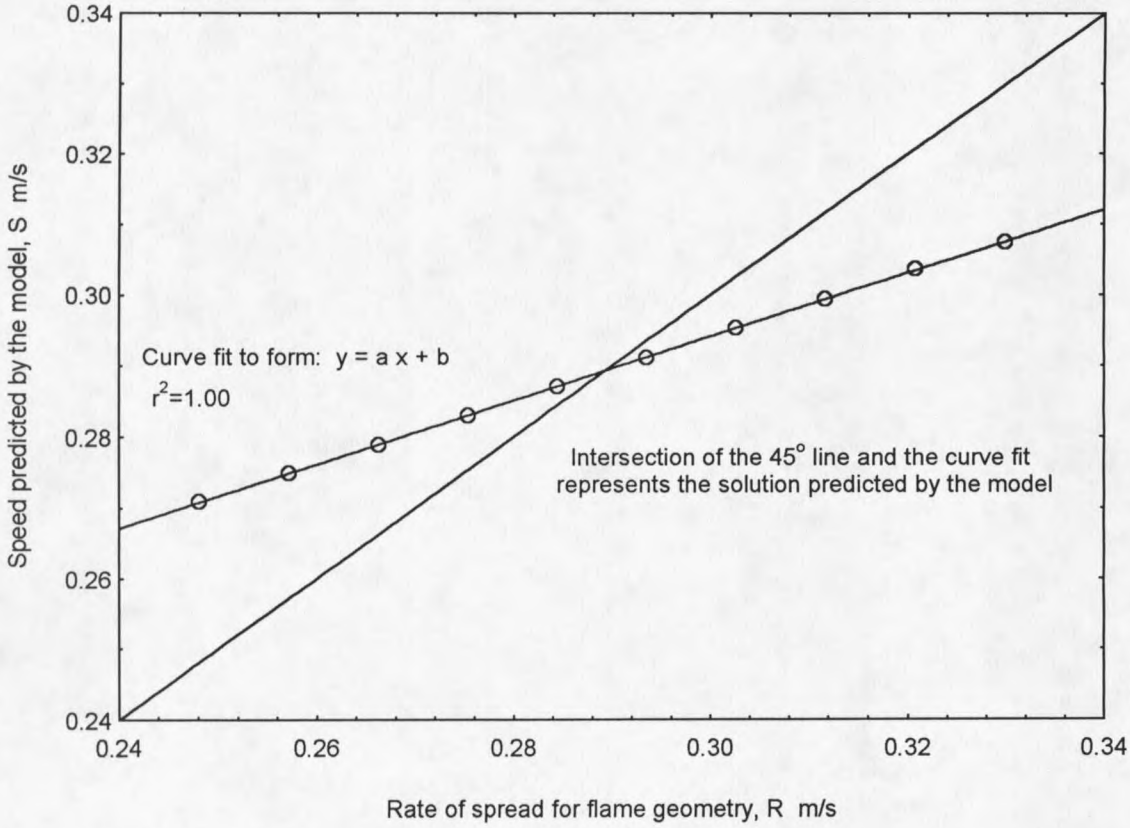

Figure C3. Curve fit for spread rate prediction for Fire 4.

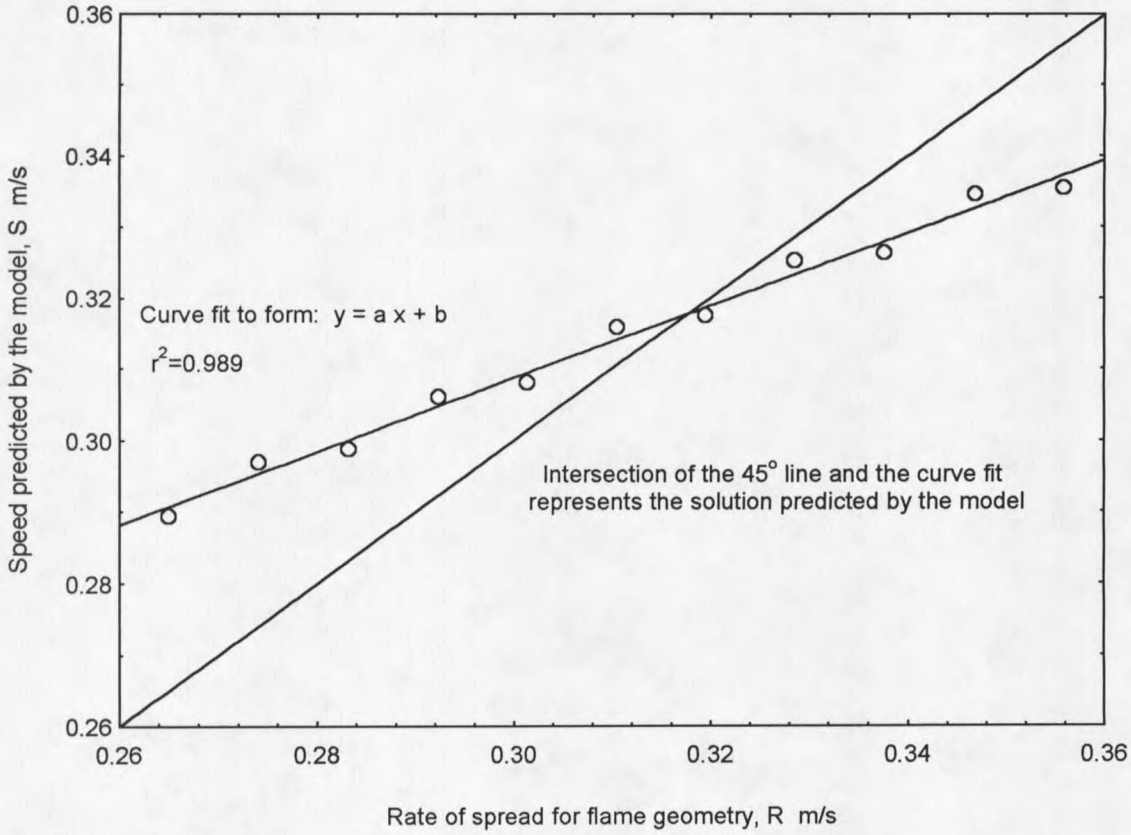

Figure C4. Curve fit for spread rate prediction for Fire 5.

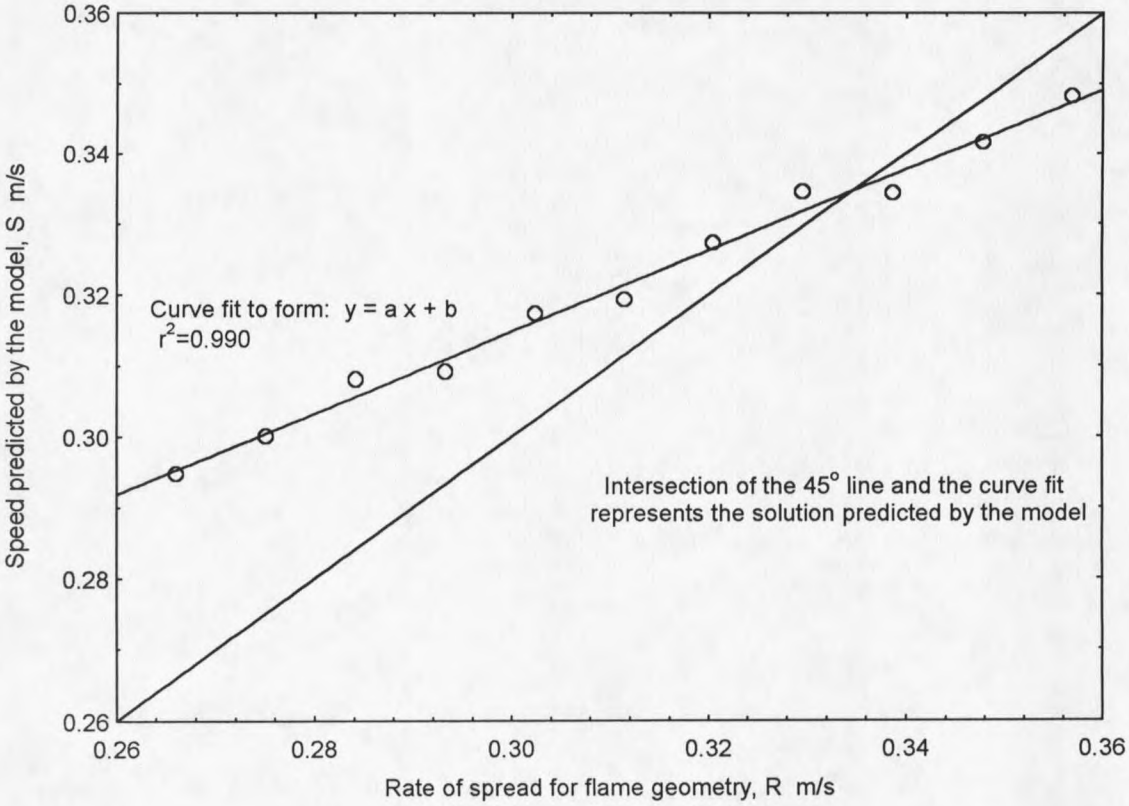

Figure C5. Curve fit for spread rate prediction for Fire 6.

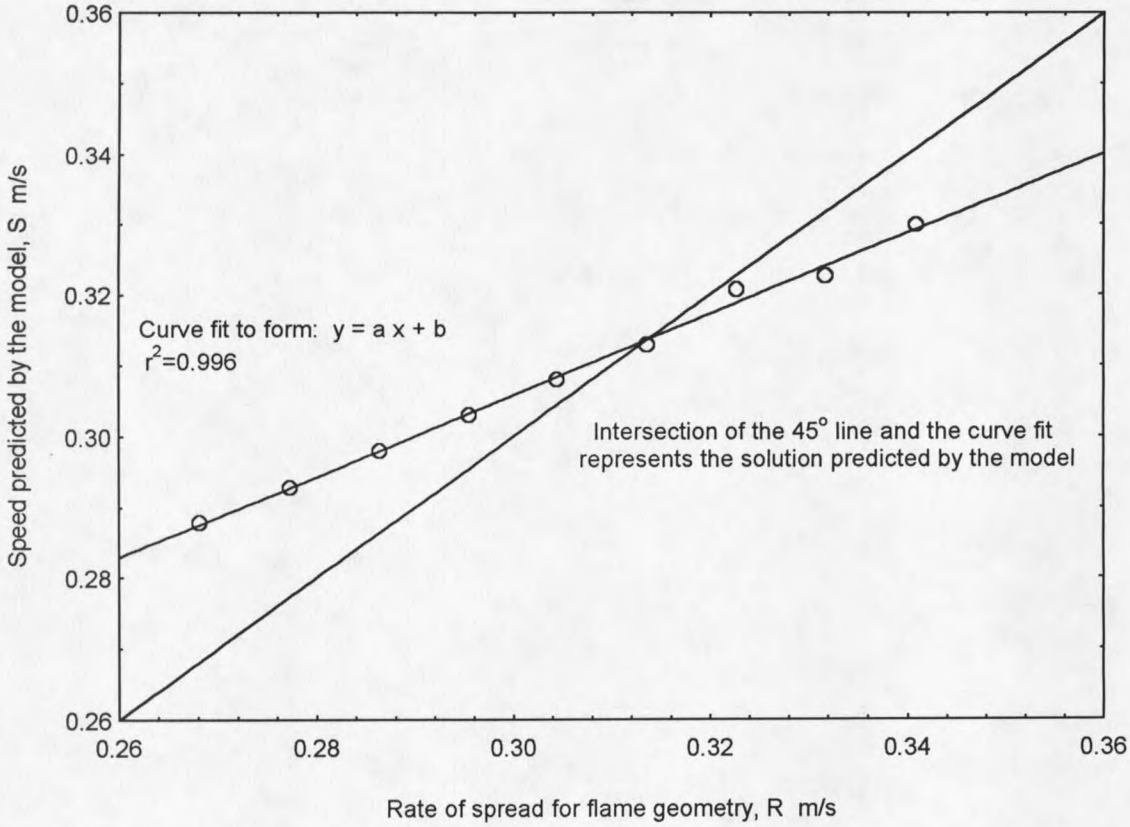

Figure C6. Curve fit for spread rate prediction for Fire 11a.

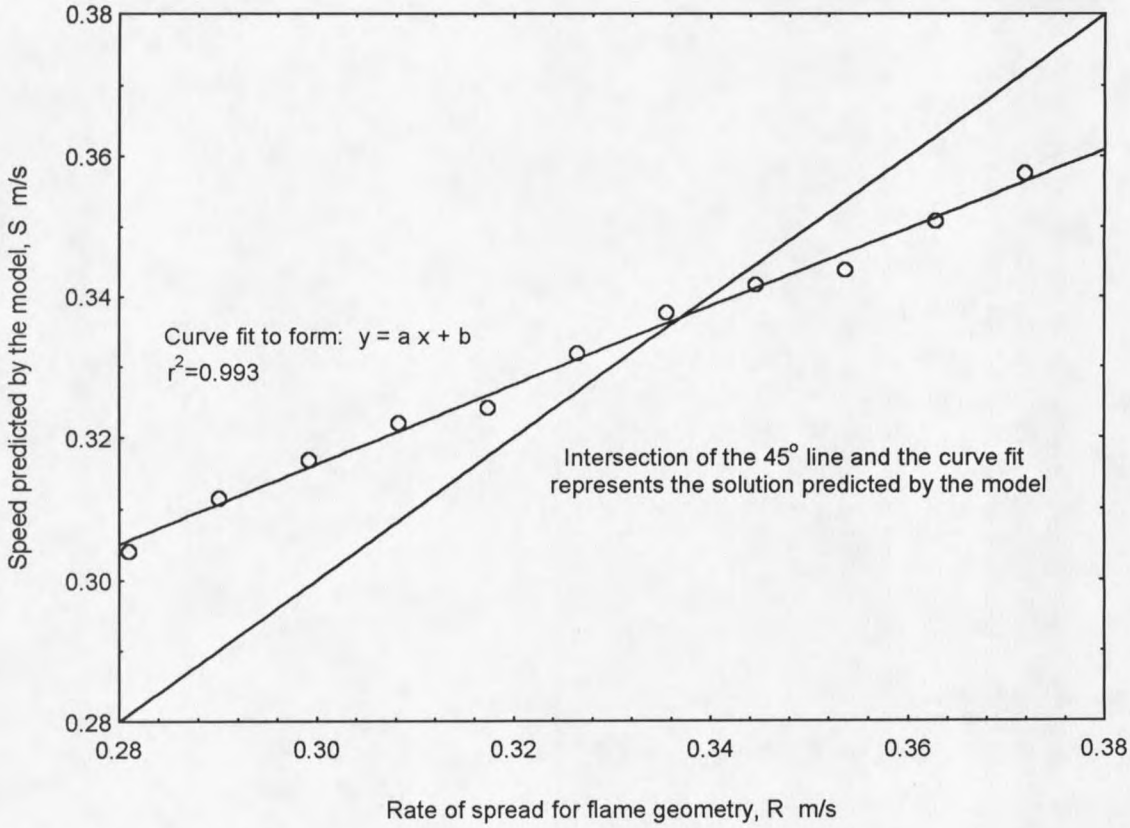

Figure C7. Curve fit for spread rate prediction for Fire 11b.

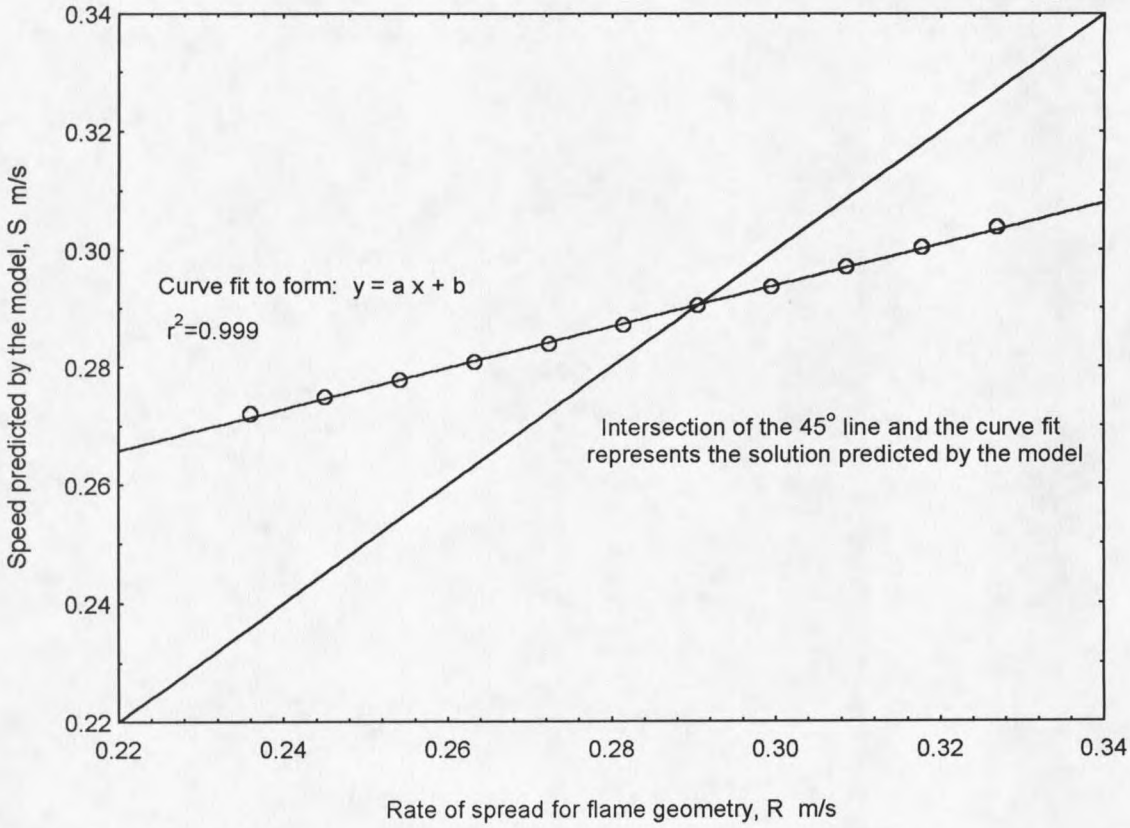

Figure C8. Curve fit for spread rate prediction for Fire 12.

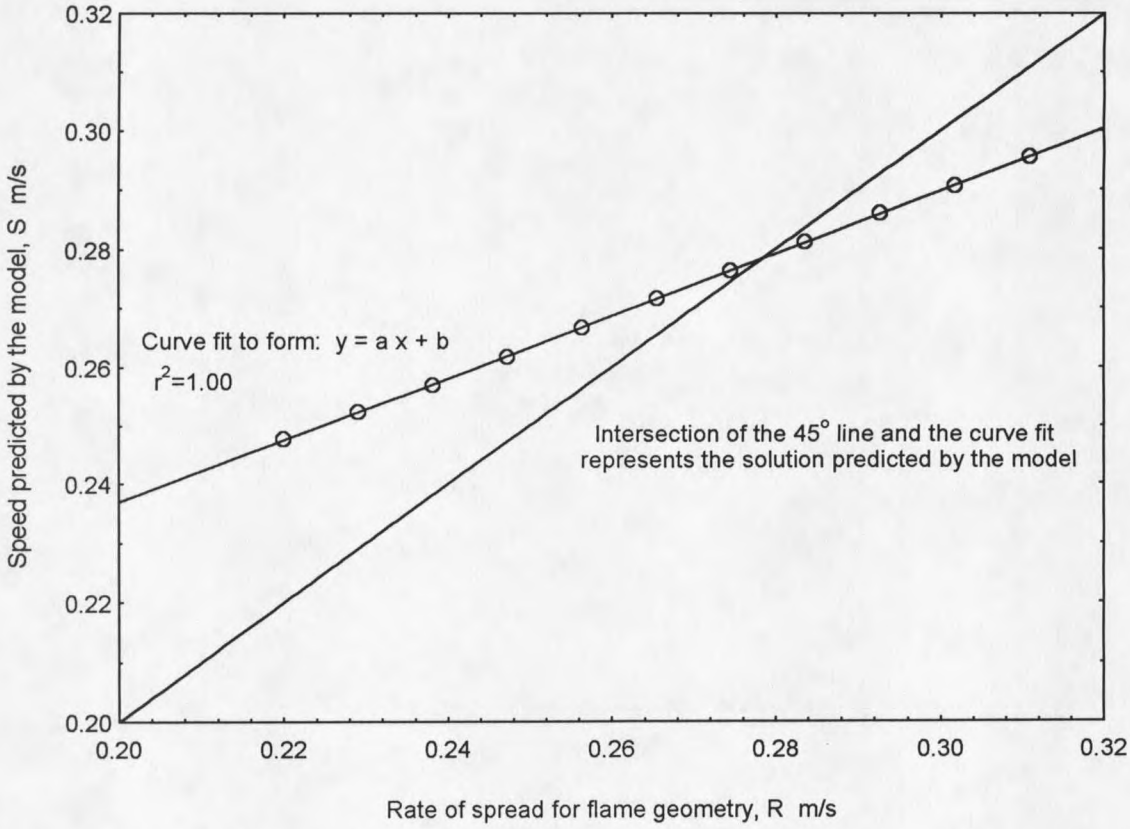

Figure C9. Curve fit for spread rate prediction for Fire 13.

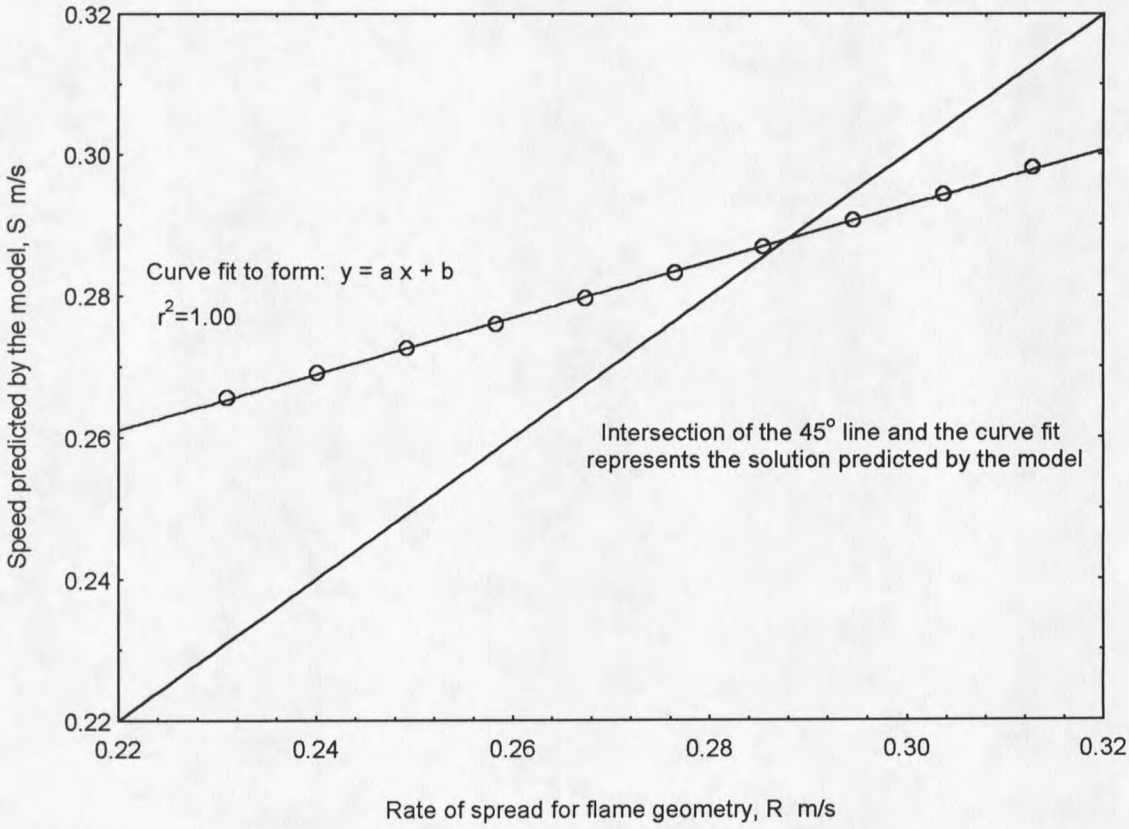

Figure C10. Curve fit for spread rate prediction for Fire 14.